Treatment of the Impacts of Transport Inflexion Points and Charge Trapping at the Surface States on Drain Current of AlGaN/GaN HFETs

Alireza Loghmany

A Thesis

in

The Department

of

Electrical and Computer Engineering

Presented in Partial Fulfillment of the Requirements

for the Degree of Master of Applied Science (Electrical Engineering) at

Concordia University

Montreal, Quebec, Canada

August 2010

© Alireza Loghmany, 2010

CONCORDIA UNIVERSITY

School of Graduate Studies

This is to certify that the thesis prepared

By: Alireza Loghmany

Entitled: Treatment of the Impacts of Transport Inflexion Points and Charge Trapping at the Surface States on Drain Current of AlGaN/GaN HFETs

and submitted in partial fulfillment of the requirements for the degree of

Master of Applied Science (Electrical Engineering)

complies with the regulations of the University and meets the accepted standards with respect to originality and quality.

Signed by the final examining committee:

Dr. D. Qiu ____________________________Chair

Dr. A. Ben Hamza, CIISE ___________Examiner

Dr. M. Z. Kabir ___________________Examiner

Dr. P. Valizadeh __________________Supervisor

Approved by Dr. W. E. Lynch ___________________________
Chair, Department of Electrical and Computer Engineering

___________20__ Dr. Robin A. L. Drew ________________________
Dean, Faculty of Engineering and Computer Science

ABSTRACT

Treatment of the Impacts of Transport Inflexion Points and Charge Trapping at the Surface States on Drain Current of AlGaN/GaN HFETs

Alireza Loghmany

During the past two decades AlGaN/GaN Heterostructure Field Effect Transistors (HFETs) have been the target of much attention in high power microwave applications. Crystal imperfections in AlGaN/GaN HFETs have been pointed out as the cause of many reliability concerns such as drain-current collapse, gate lag, and excessive gate leakage-current. Current collapse and reliability degradation due to electron trapping at the surface layer of AlGaN/GaN HFETs are major impediments for commercialization of these devices. Even though there have been remarkable improvements in crystal growth and device fabrication technology, trapping effects in AlGaN/GaN HFETs, specially under high drain-voltage conditions, have not been completely removed. Therefore, an assured simulation of HFET with incorporation of trapping effects is needed. In this thesis, in order to substantiate the hypothesis of electron trapping at deep surface states as the cause of semi-permanent current collapse this phenomenon is studied with the use of CADtool Medici.

Monte Carlo simulation of electronic transport at AlGaN/GaN channels reveals that in addition to the steady-state velocity overshoot there exists a pronounced kink in the low electric-field region of the drift-velocity versus electric-field characteristics of these channels. Existence of the inflexion points attributed to this kink and the large width of the overshoot pattern in conjunction with the large electric-fields conventionally

applied to these wide band-gap semiconductors, make the modeling of electronic devices fabricated in this technology different than those of other III-V semiconductors. An analytical model for drain current/voltage characteristic of AlGaN/GaN HFETs with incorporation of steady-state drift-velocity overshoot and the inflexion points in the electronic drift transport characteristics is also presented in this thesis. The wide peak and pronounced inflexion points in the transport characteristics of AlGaN/GaN heterojunctions are modeled through considering a drift-diffusion channel rather than a drift-only transport channel. Simulation results have been compared to a non-diffusion type channel implemented with the assumption of Ridley's saturating transport model. The model is based on applying an iterative approach between Poisson's equation and current-continuity equation, which relieves the results from the burden of the choice of fitting parameters. With the advancement of this technology, development of a versatile analytical model with incorporation of these considerations is vital for understanding the full range of capabilities of III-Nitride material system.

AKNOWLEDGEMENTS

I am indebted to many people without whom this work would not have been possible. First of all, I am deeply grateful to my supervisor, Professor Pouya Valizadeh from whom I received numerous inspirations and guidance, as well as encouragement and support. In addition, I have enjoyed the supportive and collegial atmosphere he promotes in his group.

I would like to thank other members of my research group, Mr. Maziar Moradi and Mr. Farzin Manouchehri for their support. Their encouragement, care and help made my life here enjoyable.

I would like to thank my parents for all their support. Finally, I would like to give my special gratitude to my wife and my son for their support, understanding, patience, and sacrifices.

TABLE OF CONTENTS

List of Figures viii

List of Tables xi

1 Introduction 1

1.1 III-Nitride material systems 1

1.2 AlGaN/GaN Heterostructure Field-Effect Transistor 2

1.2.1 Device structure 4

1.2.2 Polarization in AlGaN/GaN HFETs 5

1.3 Microwave performance of AlGaN/GaN HFETs 6

1.4 Reliability of AlGaN/GaN HFETs 7

1.4.1 Current collapse 8

1.4.2 Gate leakage 8

1.4.3 Leakage through substrate 9

1.5 Overview of thesis 9

2 Impacts of Charge Trapping at the Surface States on Drain-Current of AlGaN/GaN HFETs 11

2.1 Introduction 11

2.2 Medici simulation and modeling of AlGaN/GaN HFETs 14

2.2.1 Introduction to Medici 14

2.2.2 Numerical simulation using Medici 16

2.2.3 Device structure 17

2.2.4 Simulation results and conclusions 21

2.2.4.1 Before stress 21

2.2.4.2 After stress 26

3 Analytical Modeling of Drain-Current Characteristics of AlGaN/GaN HFETs with Incorporation of the Impacts of Inflexion Points and Steady-State Velocity Overshoot 32

3.1 Abstract 32

3.2 Introduction 33

3.3 Description of the model 35

3.3.1 Drain-current simulation of self-aligned HFET 38

3.3.1.1 Linear-region characteristics (i.e. $E < E_{v\text{-}max}$) 39

3.3.1.2 Saturation-region characteristics (i.e. E>$E_{v\text{-}max}$) 40
3.3.2 Drain-current simulation of non- self-aligned HFET 46
3.4 Simulation results and discussions 48
3.5 Conclusion 58
4 Conclusion and Future Works 59
4.1 Goals and contributions of the thesis 59
4.2 Conclusions 59
4.3 Future works 60
Bibliography 62
Appendix A: Material parameters redefinition of GaAs as GaN and AlGaAs as AlGaN 69
Appendix B: Medici input files of simulation 79

LIST OF FIGURES

Figure 1.1: Electron velocity versus electric-field for Si, SiC, GaAs and GaN [7]. 2

Figure 1.2: AlGaAs/GaAs HFET device structure [11]. 3

Figure 1.3: AlGaN/GaN HFET structure [11]. 4

Figure 1.4: Conudction-band diagram of AlGaN/GaN HFET...4

Figure 1.5: Schematic drawing of the crystal structure of Wurtzite Ga-face and N-face GaN [13].. 5

Figure 1.6: Spontaneous and piezoelectric polarization in AlGaN/GaN HFET [14]..........6

Figure 1.7: Historical progress in GaN-based transistors technology. (a) Power density of AlGaN/GaN HFET versus year. (b) Total power of AlGaN/GaN HFETs versus year [16]...7

Figure 2.1: Schematic cross section of the presented AlGaN/GaN HFET. Region of the surface with charge trapping is marked with the oval (figure is not in scale) 19

Figure 2.2: Schematic cross section of the presented AlGaN/GaN HFET illustrating current flow before stress for V_{GS}=0 V and V_{DS}=0.05 V.............................22

Figure 2.3: Electron concentration (cm^{-3}) of the channel under the gate-drain access region (a) and gate (b) along the direction perpendicular to device surface for V_{GS}=0 V and V_{DS}=0.05 V. Device surface is assumed to be at x=0... 24

Figure 2.4: Energy band diagram under the gate along vertical direction for V_{GS}=0 V and V_{DS}=0.05 V. Inset: The zoomed-in view of this energy-band diagram at the vicinity of the heterointerface...25

Figure 2.5: I-V characteristics of simulation result (solid line) versus experimental data (dashed line) with the assumption of L_G=0.25 μm and L_{GD}=1.875 μm for V_{GS}=-1.8 V~-3 V with the step of 0.4 V (before stress).. 26

Figure 2.6: Schematic cross section of the presented AlGaN/GaN HFET illustrating current flow after stress for V_{GS}=0 V and V_{DS}=0.05 V.................................27

Figure 2.7: Electron concentration in the channel of the device for V_{GS}=0 V (a) and V_{GS}=-3 V (b) along the longitudinal direction. V_{DS} is equal to 5 V. Source edge of the gate is assumed to be at x=0.. 29

Figure 2.8: Electric-field along the channel after stress for V_{GS}=-1.8 V and V_{DS}=5 V. Source edge of the gate is assumed to be at x=0...30

Figure 2.9: I-V characteristics of simulation result (solid line) versus experimental data (dashed line) with the assumption of R_s=0 Ω, R_d=0 Ω, L_G=0.25 μm,

and L_{GD}=1.875 μm for V_{GS}=-1.8 V~-3 V with the step of 0.4 V (after stress)..31

Figure 3.1: Drift-velocity vs. electric-field characteristic of the adopted mobility model (solid line) and Ridley's model (dashed line).. 36

Figure 3.2: Schematic cross-section of a self-aligned AlGaN/GaN HFET. Sections identified by I and II are explained in the text.. 38

Figure 3.3: Schematic cross-section of a self-aligned AlGaN/GaN HFET, illustrating the Gaussian box used in the analysis of saturation-region. The inset shows the conduction band-edge at the AlGaN/GaN heterointerface.............41

Figure 3.4: Simulation flowchart for the self-aligned AlGaN/GaN HFET.. 45

Figure 3.5: Schematic cross-section of a non- self-aligned AlGaN/GaN HFET. Sections identified by I, II, III and IV are explained in the text.. 46

Figure 3.6: Convergence of threshold voltage distribution (a), electric-field distribution (b), and diffusion current density (c) in region II after 6 steps of iteration for V_{GS}=-1.8 V, I=124 mA. Convergence is achieved to the curve shown in solid line. R_S and R_D are equal to 5 Ω..................................48

Figure 3.7: Drain I-V characteristics based on mobility model of (3.2) (solid curve) versus Ridley's mobility model (dashed curve) for V_{GS}=-1.8~-3.0 V with steps of 0.4 V for a non-self-aligned HFET (a) and a self-aligned HFET (b). R_S and R_D are equal to 5 Ω...49

Figure 3.8: Drain I-V characteristics based on mobility model of (3.2) (solid curve) versus Ridley's mobility model (dashed curve) for V_{GS}=-1.8~-3.0 V with steps of 0.4 V for a non-self-aligned HFET (a) and a self-aligned HFET (b). R_S and R_D are equal to 0 Ω...50

Figure 3.9: Drain I-V characteristics based on mobility model of (3.2) (solid curve) versus Ridley's mobility model (dashed curve) for V_{GS}=-1.8~-3.0 V with steps of 0.4 V for a non-self-aligned HFET (a) and a self-aligned HFET (b). R_S and R_D are equal to 20 Ω...51

Figure 3.10: Drain I-V characteristics based on mobility model of (3.2) (solid curve) versus Ridley's mobility model (dashed curve) for V_{GS}=-1.8~-3.0 V with steps of 0.4 V for a non-self-aligned HFET (a) and a self-aligned HFET (b). R_S and R_D are equal to 35 Ω...52

Figure 3.11: Drain I-V characteristics based on Ridley's mobility model (solid curve) versus experimental measurements (dashed curve) for V_{GS}=-1.8~-3.4 V with steps of 0.4 V. The simulated device is a non-self-aligned HFET with

R_S and R_D of 5 Ω, and L_{GD}=1.875 µm. The mismatch close to threshold voltage is due to the lack of consideration of leakage through buffer layer....53

Figure 3.12: Drain I-V characteristics based on simple Einstein's relationship (solid line) versus corrected Einstein's relationship (dashed line) for a non-self-aligned HFET with the assumption of R_S=R_D=0 Ω, L_G=0.25 µm, and L_{GD}=1.0 µm for V_{GS}=-1.8 V~-3.0 V with the step of 0.4 V. Inset: Correction factor as a function of reduced Fermi level $\eta=\frac{E_F-E_C}{K_BT}$ 54

Figure 3.13: v_d-E characteristics according to (3.2) and (3.18).......................................55

Figure 3.14: Drain I-V characteristics based on mobility model of (3.2) (solid line), versus (3.18) (dashed line) for L_G=0.25 µm (a), L_G=0.5 µm (b), and L_G=1 µm (c), for V_{GS}=-1.8~-3.0 V with steps of 0.4 V..56

Figure 3.15: Drain I-V characteristics based on mobility model of (3.2) (solid line), versus (3.18) (dashed line) for L_{GD}=1 µm (a), L_{GD}=2 µm (b), and L_{GD}=3 µm (c), for V_{GS}=-1.8~-3.0 V with steps of 0.4 V..57

LIST OF TABLES

Table 2.1: Parameters used in simulation 20
Table 3.1: Parameters used in simulation 38

Chapter 1

Introduction

1.1 III-Nitride material systems

Good transport properties, widely tunable band-gap, superb bond-strength, and high breakdown electric-field in III-Nitride semiconductors (including InN, GaN, AlN, and their ternary alloys) make them suitable for realization of high-power, high-frequency and high-temperature RF-circuitry [1], [2]. With the room temperature band-gap of 0.7 eV for InN [3] and the band-gap of 6.2 eV of AlN [4], III-Nitride alloys can cover a very broad range of band-gaps and emission wave-lengths from infrared to the deep ultraviolet, which is currently employed in the making of Light Emitting Diodes (LEDs), Laser Diodes (LDs), and photo detectors.

Suitability of the application of III-Nitride heterostructures to electronic devices is not only due to their transport properties, but also due to the polar properties of their heterostructures which allow the formation of two-dimensional channels of extremely high carrier concentrations ($\geq 10^{13}\ \mathrm{cm}^{-2}$), without the need for intentional doping. Gallium nitride (GaN) is the most investigated semiconductor of the III-Nitride material system. Although, low-field electron mobility of GaN is much less than that of GaAs (i.e. the main contender in the active microwave device market), its larger peak electron velocity,

wider velocity overshoot pattern, and higher thermal stability have been deemed sufficient for turning the table on GaAs, specially at the lower frequency ends and higher power levels [5], [6]. Figure 1.1 compares electron drift-velocity versus electric-field characteristics of GaN with two other major semiconductors (i.e. Si and GaAs), and also to SiC as another wide band-gap semiconductor.

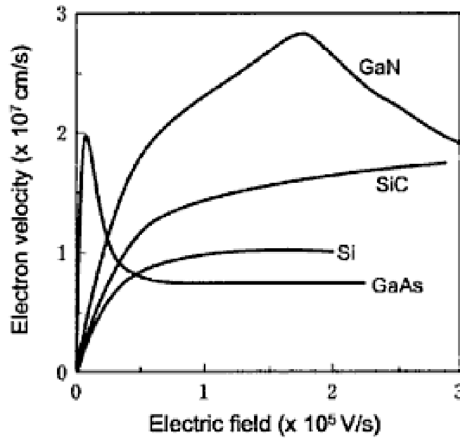

Figure 1.1: Electron velocity versus electric-field for Si, SiC, GaAs and GaN [7].

1.2 AlGaN/GaN Heterostructure Field-Effect Transistor

Heterostructure Filed-Effect Transistor (HFET) is a promising candidate for low noise microwave power applications [8], [9], [10]. A traditional AlGaAs/GaAs HFET is illustrated in Fig. 1.2. Traditional HFET technology improves the carrier mobility of two-dimensional electron gas (2DEG), formed at the vicinity of the heterointerface of the channel/buffer layer and the doped barrier, by resolving the ionized-impurity scattering problem via spatially separating the channel from these scattering sources. At the cost of reduction of the gate-transconductance, impurity scattering can be further reduced by

increasing the spatial separation of the electrons and ionized impurities through incorporation of a thin undoped spacer layer between barrier and the channel.

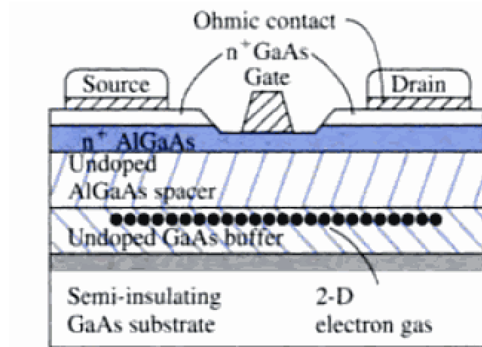

Figure 1.2: AlGaAs/GaAs HFET device structure [11].

HFETs are suitable structures for high frequency low noise amplifiers and now are widely used as extremely low noise devices in terrestrial and space telecommunications systems, space radio telescopes, Direct Broadcasting Satellite television (DBS) receivers, microwave and high power amplifiers, cellular phones and car navigation receivers.

Over the past two decades, AlGaN/GaN HFETs grown on sapphire and SiC have demonstrated much larger output power and temperature tolerance than AlGaAs/GaAs HFETs, which were previously the primary HFET candidates for high power applications. This is primarily due to the application of wider band-gap materials and the ability to achieve outstanding 2DEG densities without the need for intentional doping of the barrier in the polar AlGaN/GaN heterostructures. The first AlGaN/GaN HFET was demonstrated by Khan *et al.* in 1994 [12].

1.2.1 Device structure

Figure 1.3 shows the typical device structure of an AlGaN/GaN HFET. Not unlike AlGaAs/GaAs HFETs, in these structures due to difference in energy band-gap of the two materials forming the heterojunction, there is a band-gap discontinuity at the heterointerface. This discontinuity creates a triangular quantum well which leads to the formation of a two-dimensional electronic channel in the undoped GaN. However, unlike AlGaAs/GaAs HFETs existence of strong polarization at the heterointerface of AlGaN/GaN HFETs causes an extra band-bending and reversal of the curvature of barrier's conduction band-edge which result in boosting the 2DEG concentration even in absence of intentional barrier doping [6]. Figure 1.4 shows the conduction-band diagram of AlGaN/GaN HFET.

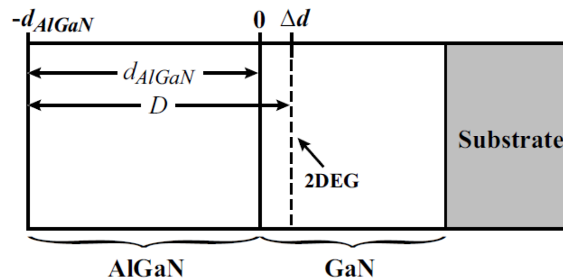

Figure 1.3: AlGaN/GaN HFET structure [11].

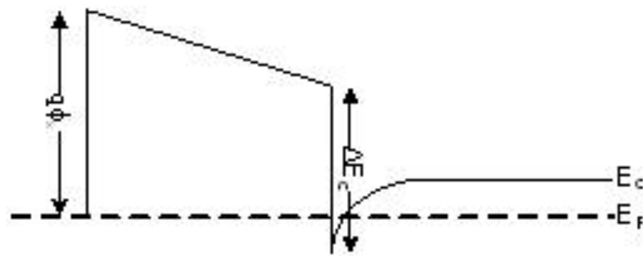

Figure 1.4: Conduction-band diagram of AlGaN/GaN HFET.

1.2.2 Polarization in AlGaN/GaN HFETs

III-Nitrides semiconductors can be grown in two different crystalline forms: Zinc blende (Zb) and Wurtzite (Wz). Wurtzite which is the most common structure in III-Nitride materials has a hexagonal structure as shown in Figure 1.5 [13]. Non-centro-symmetric nature of Wurtzite structure leads to formation of spontaneous polarization in III-Nitrides even in absence of external strain and/or electric-field.

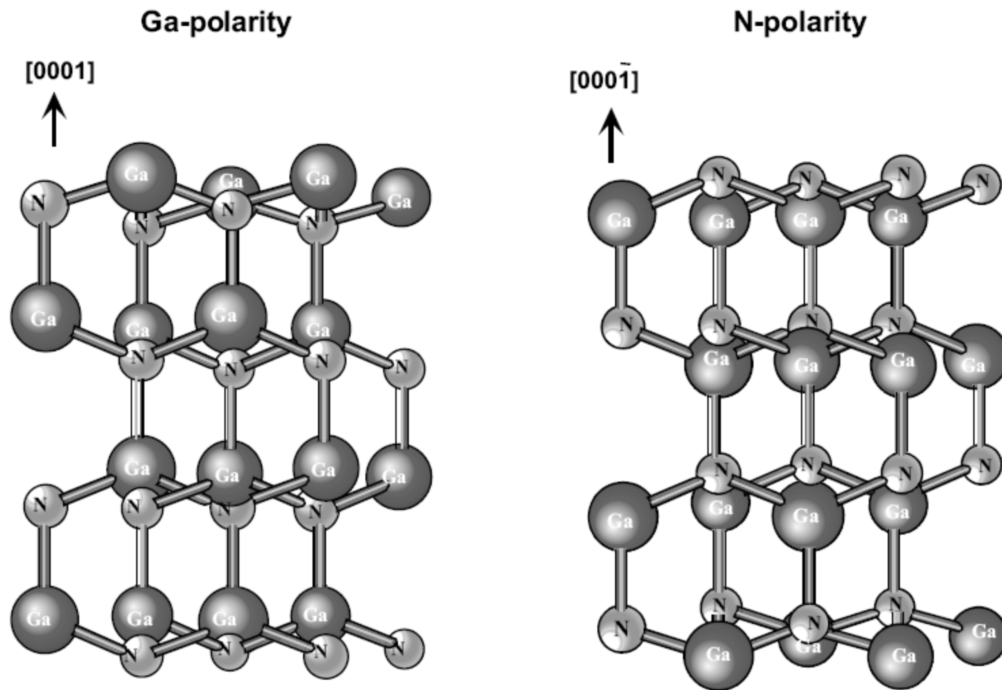

Figure 1.5: Schematic drawing of the crystal structure of Wurtzite Ga-face and N-face GaN [13].

Furthermore, a sizable piezoelectric polarization term exits in the strained pseudomorphically-grown III-Nitride heterojunctions. This is due to induction of strain through coherent growth of two lattice-mismatched crystals and the large value of piezoelectric coefficients of the III-Nitride material system [6]. Piezoelectric effect in addition to the difference between spontaneous polarization of GaN channel and AlGaN

barrier-layer causes the formation of a sizable polarization sheet charge at the AlGaN/GaN heterointerface. Figure 1.6 shows the spontaneous and piezoelectric polarizations in the AlGaN/GaN HFET [14]. In this figure, spontaneous polarization in each material is shown as P_{sp} and piezoelectric polarization in the tensile-strained AlGaN barrier is represented by P_{pz}. The value of spontaneous polarization increases along the material order of GaN to AlN, and to InN [4], [6].

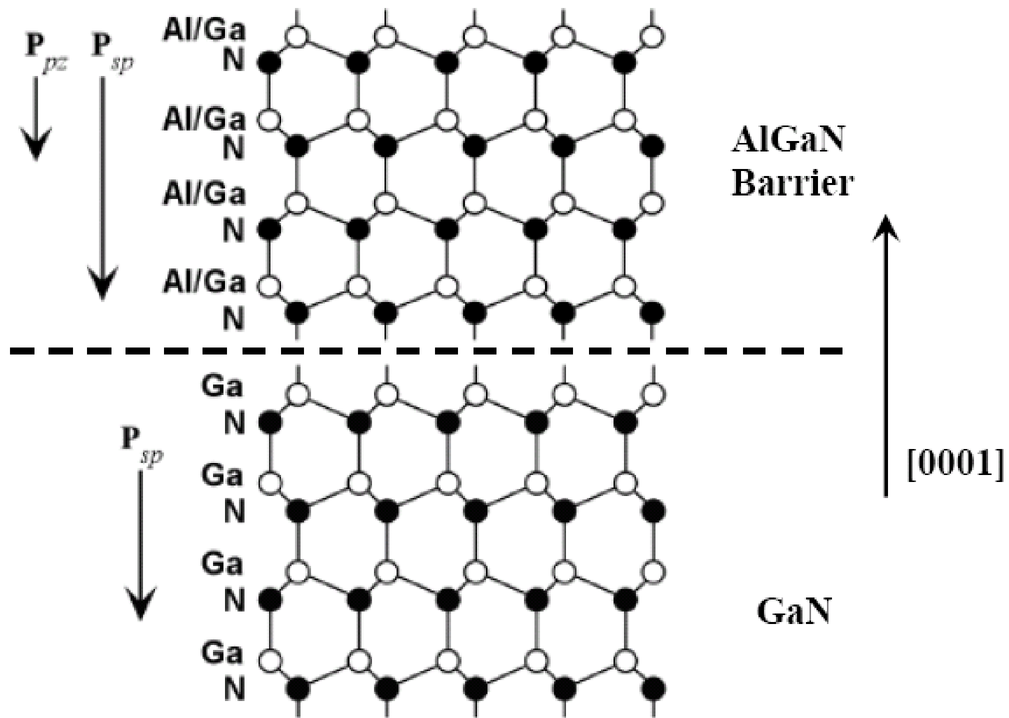

Figure 1.6: Spontaneous and piezoelectric polarization in AlGaN/GaN HFET [14].

1.3 Microwave performance of AlGaN/GaN HFETs

Due to high breakdown voltage of AlGaN/GaN HFETs, these transistors can be operated under high drain-voltages and high peak efficiencies satisfying the needs of commercial systems such as wireless base stations. Over the years, significant progress has been

made in terms of power density and total available power of AlGaN/GaN HFETs. Figure 1.7 shows the historical progress diagram of GaN-based transistors during their first few years of development. Recently, Cree Inc. has reported GaN based transistors with output power of 240 W and gain of 11.5 dB for S-band (i.e. 2-4 GHz) applications [15].

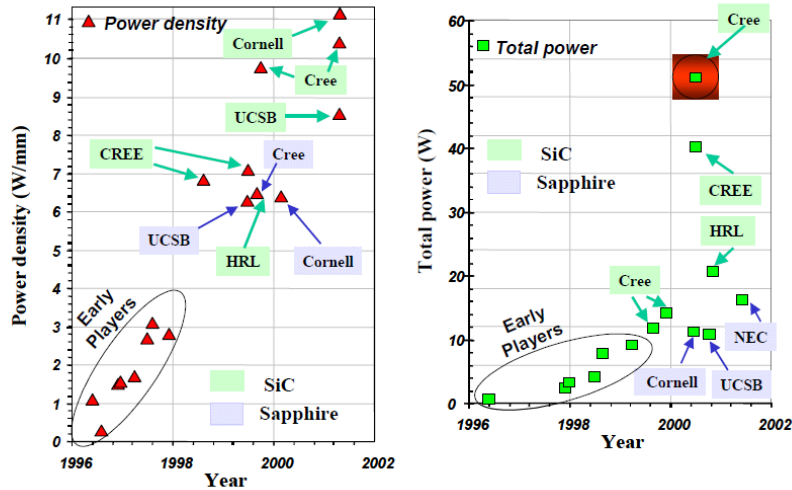

Figure 1.7: Historical progress in GaN-based transistors technology. (a) Power density of AlGaN/GaN HFET versus year. (b) Total power of AlGaN/GaN HFETs versus year [16].

1.4 Reliability of AlGaN/GaN HFETs

Although AlGaN/GaN HFET is a promising device for high power applications, at the present time the key issue which prevents this transistor from being fully commercialized is the issue of long-term reliability. The main reliability concerns of AlGaN/GaN HFETs are drain-current collapse, gate leakage, and leakage through substrate.

1.4.1 Current collapse

The microwave output power of an AlGaN/GaN HFET has been observed to considerably deteriorate after long-term application of large DC voltages or under nominal microwave operating conditions [17], [18]. It has been speculated that these stressing schemes lead to the injection of hot carriers from the channel to the deep surface states in the high electric-field regions of the channel [18]. Trapping of these hot carriers leads to reduction in drain current of the device, which consequently degrades the microwave output performance. This phenomenon is referred to as current collapse or current slump and is described further in chapter 2.

Through improvement of crystalline quality of the HFET structure and electrically satisfying the surface traps by incorporation of a surface passivation layers it has been attempted to reduce these effects [19], [20]. Silicon nitride passivation has been shown to possess the ability of reducing the effects of these surface states [20-25]. Recently, a new technique has been investigated to suppress the current collapse by using polycrystalline AlN passivation layer [26]. The larger thermal conductivity of AlN, is also enticing due to its capability of boosting the maximum operating conditions dictated by the channel temperature [26], [27], [28].

1.4.2 Gate leakage

High gate leakage-current is another drawback for AlGaN/GaN HFETs which should be reduced to suppress their power consumption and noise. Mechanisms of gate leakage current of these devices are not fully understood yet. Different mechanisms such as trap-

and defect-assisted tunnelling, barrier-thinning caused by charge trapping, and hopping through dislocations among others have been counted responsible for this excessive gate leakage. According to these explanations, existence of a distributed band of traps located within the barrier height of the AlGaN barrier acts as the facilitator in tunnelling through the barrier [29], [30], [31]. Surface roughness has also been shown to be a major player in this regard [32].

1.4.3 Leakage through substrate

Lattice mismatch and difference between thermal expansion coefficients of epitaxially-grown III-Nitride layers and common substrates such as sapphire, Si, and SiC lead to high defect densities within these structures [13]. This is a limiting factor on the performance of these devices. The impacts of these imperfections are often observed in terms of unintentional doping of the buffer layer which results in soft pinch-off and leakage through this layer. Better device performance is expected when using the lattice-matched GaN substrate. Commercially available GaN substrates are currently being grown by Hydride Vapour Phase Epitaxy (HVPE) [33], [34]. However, still on these substrates presence of oxygen impurities causes n-type conductivity and substrate leakage. Transition metal doping can be used to change the conductive substrate into a semi-insulating substrate which can suppress the leakage current though substrate [35].

1.5 Overview of thesis

Current collapse is one of the most important reliability concerns of AlGaN/GaN HFETs,

which degrades the output performance of the device. Thus, incorporation of the impacts of the surface trap states in modeling these devices is vital. Furthermore, incorporation of full transport characteristics of GaN plays an important role in modeling these devices. My motivations for this study have been the incorporation of these features in an analytical model.

In chapter 2 of the thesis an assured simulation of AlGaN/GaN HFET including the impact of electron trapping at deep surface states with the use of CADtool Medici® is performed. Medici® in its present form is not programmed for modeling the behavior of polar GaN based heterostructures, as a result material parameters of GaN and AlGaN and polarization terms are manually defined and can be found in appendix A.

In chapter 3, an analytical model for drain-current characteristic of AlGaN/GaN HFETs with incorporation of inflexion points and steady-state velocity overshoot is presented. The wide peak and pronounced inflexion points in the transport characteristics of AlGaN/GaN heterojunctions are modeled through considering a drift-diffusion channel rather than a drift-only transport channel. Simulation results have been compared to a non-diffusion type channel implemented with the assumption of the transport model in which manifestations of these transport characteristics have been neglected. The proposed model is based on applying an iterative approach between Poisson's equation and current-continuity equation. This relieves the results from the burden of the choice of fitting parameters.

Conclusions of this work and some suggested future works are presented in chapter 4.

Chapter 2

Impacts of Charge Trapping at the Surface States on Drain-Current of AlGaN/GaN HFETs

2.1 Introduction

GaN crystals suffer from a large variety of imperfections caused by contributing factors such as residual impurities [36] and presence of screw and threading dislocations among other factors [37]. The major cause of these non-idealities is the lack of a viable native substrate. While GaN substrates are currently being developed, the small size of these substrates has so far prevented them from becoming commercially viable [16], [38], [39], [40]. The lattice mismatch between GaN and commercially used substrates of this technology, such as SiC, sapphire, and Si, is the main reason for the defect formation in AlGaN/GaN HFETs. Lattice mismatch for GaN on SiC, sapphire, and Si are 3.5%, 14.5%, and 17%, respectively [41].

Crystal imperfections have been pointed out as the cause of many reliability concerns in this technology such as drain-current collapse, gate lag, and excessive gate leakage current. Drain-current of these devices is often observed to either lag behind the gate pulse (which is referred to as gate lag) or to undergo a collapse after application of bias and/or microwave signal to the gate (which is referred-to as current collapse). Current collapse and reliability degradation due to electron trapping at the surface layer of AlGaN/GaN HFETs are major impediments for commercialization of AlGaN/GaN HFETs [42].

Current collapse is a trap-related phenomenon which was first reported in an AlGaN/GaN HFET grown on a sapphire substrate by Khan *et al.* [43]. Current collapse reduces the maximum drain-current and increases the knee voltage often after the application of a high drain-source bias. This phenomenon leads to reduced microwave output power performance of the device [44], [45]. Hot carrier migration from the channel to surface and trapping at deep acceptor-type surface states is often discussed as one of the causes of drain current collapse of AlGaN/GaN HFETs [46]. Trapping of hot carriers can also happen at the AlGaN/GaN interface or within the GaN buffer [47]. To reduce the extent of current collapse, it has been shown that by properly introducing a surface passivation layer, current collapse can be significantly reduced [24], [25], [26], [27]. This is indicative of the role of surface traps of the gate drain access region in this process [48].

Due to negative charging of the acceptor-type surface states, surface potential in the gate-drain access region becomes negative, which leads to a loss of carriers concentration in the channel and eventually results in extension of the gate depletion

region [48], [49]. This phenomenon can be seen as the creation of a virtual secondary gate in tandem with the main gate of an HFET. In this analogy, electron accumulation in trap centers forms a negatively biased virtual gate in the drain access region immediately after the gate electrode. Pinching impact of this virtual gate on the channel causes the drain-current to reduce. The potential of this virtual gate is decided through the concentration of trapped charges in the surface of the gate-drain access region. In this case drain-current is controlled not only by the applied voltage to the metallic gate but also by the charge trapping/de-trapping process of the virtual gate.

Depending on the energy depth of these surface state, it has been reported that current collapse can either be a transient (i.e. due to shallow traps), or a semi-permanent phenomenon (i.e. due to deep traps) [17], [50]. In the first form, it has been observed that depending on the frequency response of these transients, they can have very decisive impacts on extensively reducing the microwave power gain of AlGaN/GaN HFETs through shrinking their dynamic load line while having almost no impact on their DC current characteristics [51].

Even though there have been remarkable improvements in crystal growth and device fabrication technology, trapping effects in AlGaN/GaN HFETs, under high drain voltage conditions, have not been completely removed. Therefore, an assured simulation of HFET including trapping effects is needed. In this part of the thesis, impact of electron trapping at deep surface states which is based on a steady-state model is studied with the use of CADtool Medici®.

2.2 Medici simulation and modeling of AlGaN/GaN HFETs

This chapter is focused on simulating the drain current-voltage characteristics of AlGaN/GaN HFET with the use of CADtool Medici. These characteristics are studied with and without consideration of charge trapping at the surface of drain access region. Medici is a two-dimensional numerical based device simulator from Synopsys [52]. While this software in its present form is not programmed for modeling the behaviour of polar AlGaN/GaN heterostructures, the polarization terms and other material parameters of GaN and AlGaN are manually defined by incorporating fixed charge concentrations at the surface and the heterointerfaces and also by replacing the material parameters of AlGaAs/GaAs system with those of AlGaN/GaN. The definition of polarization through incorporating layers of fixed charge at surface and heterointerface is performed according to the reported strategy of Ambacher *et al.* [53]. Appendix A of the thesis contains the material-parameter files used for the re-definition of AlGaAs/GaAs system with AlGaN/GaN parameters. These data are chosen from semiconductor characteristics data base of the Ioffe Physico-Technical Institute [4].

2.2.1 Introduction to Medici

Medici, through numerically solving of Poisson, current-continuity, and transport equations, models the two-dimensional (2D) distributions of potential and carrier concentrations in a device and can be used to predict the electrical characteristics for

arbitrary bias conditions [52]. In a Medici simulation through the definition of the following parameters a 2D device is represented:

- Mesh definition with regards to cross-sectional dimensions of the device.
- Definition of the doping types and profile in each region.
- Contact placement with regard to mesh point.
- Definition of metal work function.
- Definition of charge trapped profiles.
- Recalling the appropriate mobility model with regard to the expected type of simulation.
- Defining the tolerance for convergence.
- Application of bias and generation of the desired output characteristics.

In representing the polar AlGaN/GaN HFETs, as it was mentioned earlier, a few more steps should be taken in order to define a device:

- Define a fixed charge layer to have appropriate polar 2DEG electron concentration at AlGaN/GaN heterointerface.
- Re-define the parameters of another material system such as AlGaAs/GaAs to represent AlGaN/GaN, by recalling the material parameters for their binaries.

In order to guarantee the convergence of the numerical simulation, denser grid points should be defined in areas that electric-field has the greatest variation. In a FET, this happens at the drain edge of the gate.

The other deficiency of Medici is in defining Ohmic contacts to an AlGaN/GaN HFET. This is partly due to the lack of concrete information on the tunnelling behaviour of AlGaN. The other contributing factor is that the Ohmic contacts of III-V technologies,

unlike silicon, rather than being of tunnelling type are created through alloy formation caused by Rapid Thermal Annealing (RTA). Full representation of this chemical process is not possible in Medici. However, assumption of a highly doped GaN layer between the metallic contacts of source and drain and AlGaN barrier is assured enough for the definition of Ohmic contacts. The device structure is further elaborated in section 2.2.3.

2.2.2 Numerical simulation using Medici

After defining the mesh for every grid point a set of fundamental semiconductor equations (i.e. Poisson's equation, current-continuity equations, and transport equations) will be solved. The electric behaviour of the device is governed by Poisson's equation (2.1) and continuity equations (2.2 and 2.3):

$$\nabla^2\varphi = -\nabla . \mathrm{E} = -\frac{\rho}{\varepsilon} = -\frac{q}{\varepsilon_s}(p - N_A^- - n + N_D^+) \tag{2.1}$$

where φ, E and ρ are intrinsic Fermi potential, electric-field, and charge density, respectively. In this equation q is the charge of an electron, ε_s is the permittivity of the semiconductor, p and n are free hole and electron concentration, N_A^- and N_D^+ are the acceptor and donor ionized impurity concentrations. The continuity equations are given by:

$$\frac{\partial n}{\partial t} = \frac{1}{q}\vec{\nabla}.\overrightarrow{J_n} - (R_n - G_n) \tag{2.2}$$

$$\frac{\partial p}{\partial t} = -\frac{1}{q}\vec{\nabla}.\overrightarrow{J_p} - \left(R_p - G_p\right) \tag{2.3}$$

G and R are generation and recombination rates, respectively (subscripts n and p refer to electrons and holes). J_n and J_p are the current density of electrons and holes, respectively. Transport equations based on Boltzmann's transport theory are expressed by:

$$\overrightarrow{J_n} = q\mu_n \overrightarrow{E_n} n + qD_n \vec{\nabla} n \quad (2.4)$$

$$\overrightarrow{J_p} = q\mu_p \overrightarrow{E_p} p - qD_p \vec{\nabla} p \quad (2.5)$$

where μ_n and μ_p are the electron and hole mobilities and D_n and D_p are the electron and hole diffusion coefficients, respectively. Through self-consistent numerical solution of these equations according to the finite element technique, the current characteristic of each electrode, electric-field, and band diagram at any given location across the device can be plotted among any number of other electrical parameters [52].

In this simulation, an AlGaN/GaN HFET has been investigated under two situations: (1) Before stress and (2) After stress. It has been attempted to re-produce the experimental observation of Valizadeh *et al.* [46] concerning the role of electron trapping of hot carriers at the surface states in semi-permanent collapse of drain-current. Their observations on electron trapping, resulted by long-term bias stressing, were supported by the recovery of drain current only upon illumination of the surface of HFETs with UV light [54]. Electron de-trapping from the surface states is caused by the energizing impact of the UV light. Because of the deep energy level of these observed traps, they had not observed any recovery in room light which has a low UV content [55].

2.2.3 Device structure

Although in polar AlGaN/GaN HFETs barrier doping unlike other III-V HFETs is not required [53], presence of moderate levels of unintentional doping (i.e. in the order of high 10^{15} cm^{-3}) in the barrier and GaN buffer will leave their signatures on the device characteristics such as sub-threshold current and output resistance. As a result, in order to

provide the best match to the experimental drain current-voltage characteristics, experimentation with a range of unintentional doping levels has been carried out.

In addition, in definition of fixed polar charge layers at the heterointerface, fine tuning of the charge concentration have been required to provide the best match. The key point in this definition is avoiding the pinning of Fermi level due to the high concentration of these 2D charge concentrations.

The other factor that requires tuning is the thickness of the buffer layer. While, the maximum number of grid point in Medici is 2400, the scale difference between the thick buffer layer (i.e. of micron size) and region of the device with highest variation of electric-field (i.e. of nano size) prevents us from having sufficient number of point in the buffer layer, if the full thickness of it is considered. To avoid this issue, a balance needs to be maintained between the reduced thickness of this layer in simulation and reduction of its doping level from what these values are in reality. This will essentially maintain the same resistance between the channel and the back contact of the device.

Different devices have been investigated to create the best agreement with the experimental results. The experimental results have been borrowed from the work of Valizadeh *et al.* [46]. As shown in Figure 2.1, the device structure is defined by a 0.68 µm thick GaN buffer/channel layer, followed by a 2.5 nm AlGaN spacer layer, and a 15 nm AlGaN barrier layer. In definition of polar charge at the GaN-side of the AlGaN/GaN heterointerface, rather than a 2D sheet charge a more assured Gaussian profile is defined to incorporate also the impact of quantum capacitance [56]. Effective thickness of 2DEG is assumed to be 2 nm [57]. The device has a gate length (i.e. L_G) of 0.25 µm and gate

width (i.e. W) of 200 μm. The gate to drain spacing (i.e. L_{GD}) and gate to source spacing (i.e. L_{GS}) are 1.875 μm and total length of the device is assumed to be 25 μm. Most of this length is provided to create acceptable drain and source Ohmic contacts to the 2DEG. Figure 2.1 shows a cross sectional view of the simulated device with source, gate and drain on top. Table I shows the device parameter used in simulation, unless identified otherwise.

According to the predictions of Valizadeh *et al.* [46], charge trapping at the surface states of the gate side of drain access region is responsible for reduction of drain-current upon bias stressing. This region is also identified on Figure 2.1. Trapping parameters that are later used in this chapter for inclusion of this effect are identified in Table 2.1. In this table the values for body doping, body thickness, delta doping, channel doping, barrier doping, trap layer thickness, trap layer length, trap layer doping, trap concentration are chosen on trial and error basis.

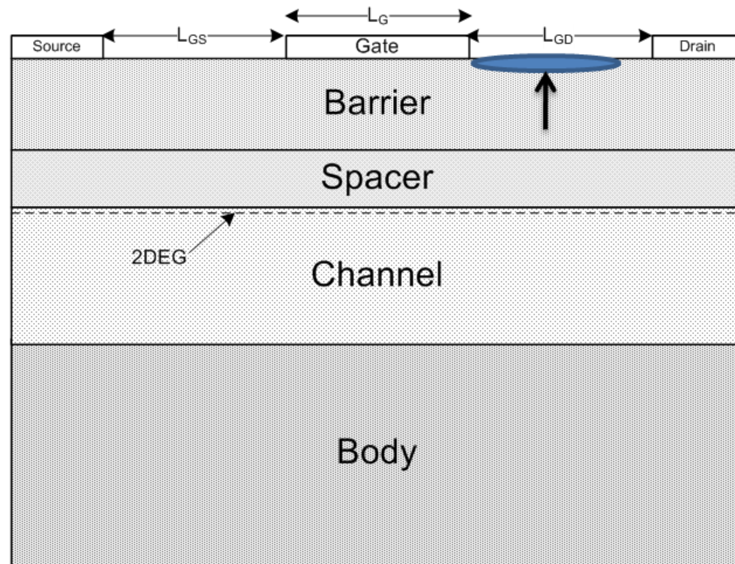

Figure 2.1: Schematic cross section of the presented AlGaN/GaN HFET. Region of the surface with charge trapping is marked with the oval (figure is not in scale).

Table 2.1: Parameter used in simulation.

Simulation parameter	Value
Body thickness	0.68 µm
Channel thickness	0.002 µm
Barrier thickness	0.015 µm
Spacer thickness	0.0025 µm
Channel length	0.25 µm
Total length	25 µm
Gate drain spacing	1.875 µm
Body doping	10^{5} cm^{-3}
Channel doping	10^{15} cm^{-3}
Barrier doping	$6\text{x}10^{17}$ cm^{-3}
Spacer doping	10^{16} cm^{-3}
Maximum 2DEG electron concentration	10^{13} cm^{-2}
Delta doping	$3.1\text{x}10^{20}$ cm^{-3}
Trap layer thickness	0.011 µm
Trap layer length from gate-edge	0.056 µm
Trap layer doping	10^{15} cm^{-3}
Trap concentration	$5.5\text{x}10^{14}$ cm^{-2}
Gate metal work function	5.17 eV

As it was mentioned earlier in chapter 1, due to spontaneous and piezoelectric polarization effects, a high concentration 2DEG exists at the AlGaN/GaN interface even without intentional doping of the barrier. In order to take this effect into account and have an assured prediction of the drain current characteristic of the device, a fixed positive sheet charge profile at the barrier side of the AlGaN/GaN heterointerface has been defined in conjunction with the 2DEG which is defined at the GaN side of this heterointerface. Density of the positive fixed charge is assumed to be 1×10^{13} cm^{-2}.

In this simulation, a longitudinal field dependent mobility is used. This is done by using "Analytic" expressions for the drift-velocity as a function of the electric-field in the direction of current flow (i.e. $E_{||}$) which is given by:

$$\mu(E_{||}) = \frac{\nu(E_{||})}{E_{||}} \tag{2.6}$$

A "gallium arsenide-like" mobility model is used with the use of appropriate changes in electron transport parameters to provide the maximum similarity with GaN electric-field vs. drift-velocity relationship [52]. These parameters have been redefined through importing the two input files of Appendix A to Medici. These data are taken from the database of Ioffe Physico Technical Institute [4].

2.2.4 Simulation results and conclusions

Medici input files of these simulations are provided in appendix B. File 1 has been used for simulating the fresh output characteristics and file 2 is used for simulation of the output characteristics of the stressed device.

2.2.4.1 Before stress

Figure 2.2 illustrates the cross sectional view of the device simulated by Medici including the current flow of the device before stress for a set of V_{GS} and V_{DS} values. The inset of this figure, illustrates a magnified view of the current flow lines in the 2DEG channel. Compression of flow lines in the 2DEG and not in the barrier and buffer layer is indicative of the acceptable formation of an HFET channel. This simulation is run by the use of input file 1, which is reported in Appendix B.

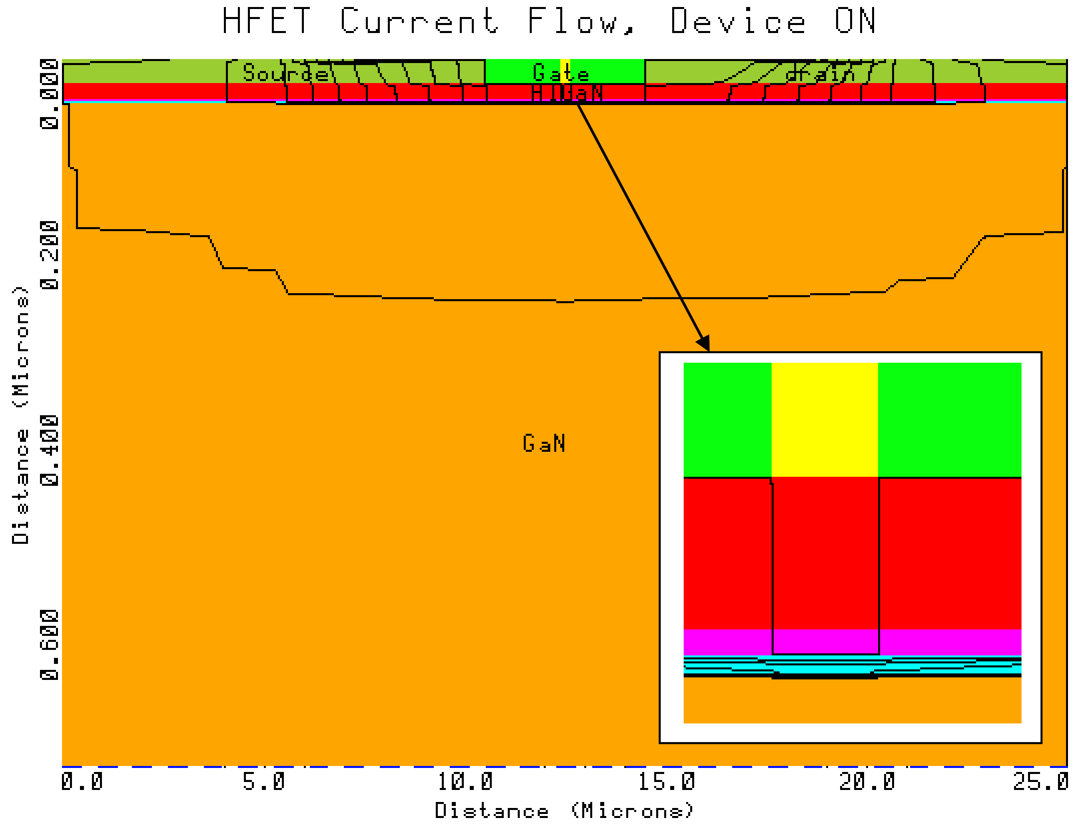

Figure 2.2: Schematic cross section of the presented AlGaN/GaN HFET illustrating current flow before stress for V_{GS}=0 V and V_{DS}=0.05 V.

In support of the formation of an HFET-type channel at AlGaN/GaN heterointerface, Figure 2.3 show the electron concentrations in the channel under the gate-drain access region (a) and gate electrode (b) along the direction normal to the heterointerface. These concentrations are provided at the same bias points as the data of Figure 2.2. Reduced peak of concentration in Figure 2.3(b) is indicative of the depleting effect of the metal gates. Oftentimes, by shrinking the thickness of the barrier, this depletion effect of the Schottky barrier on 2DEG charge is used to turn the normally depletion-type (i.e. negative threshold voltage) characteristics of AlGaN/GaN HFETs to enhancement type (i.e. positive threshold voltage) [58].

Unlike inversion type n-Metal Oxide Semiconductor Field Effect Transistor (n-MOSFET), the channel of an HFET is not normally formed due to the positive biasing of the gate. The origin of the channel charge concentration in HFETs is either the modulation doping or for the case of AlGaN/GaN HFET is the polarization nature of the heterointerface. As a result, HFETs are normally “on” at zero gate voltage (i.e. depletion-type), unless the 2DEG is depleted either by the depleting effect of the gate Schottky contact or engineering of the polarization terms and barrier doping.

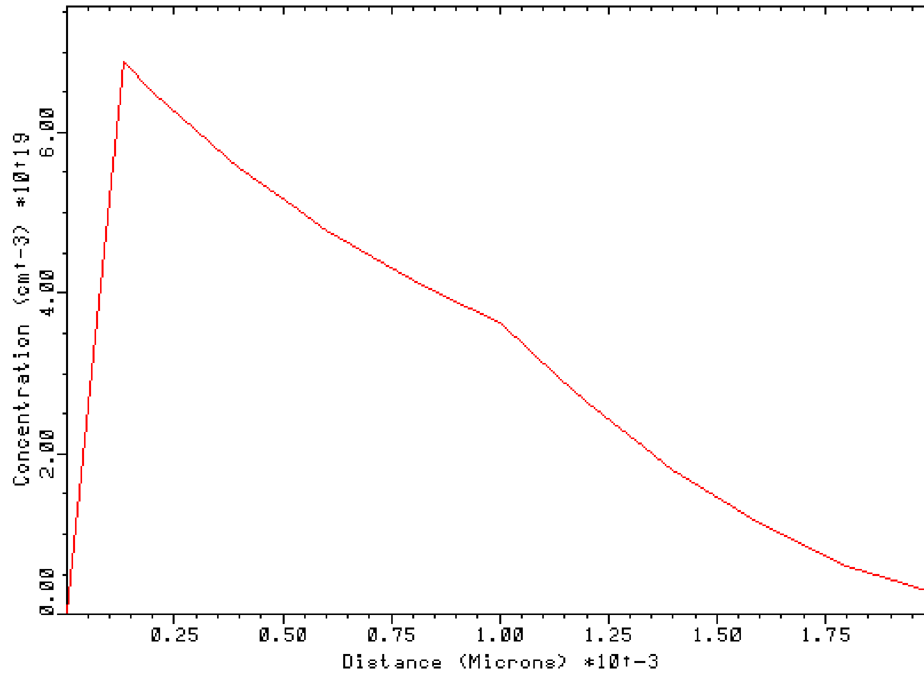

(a)

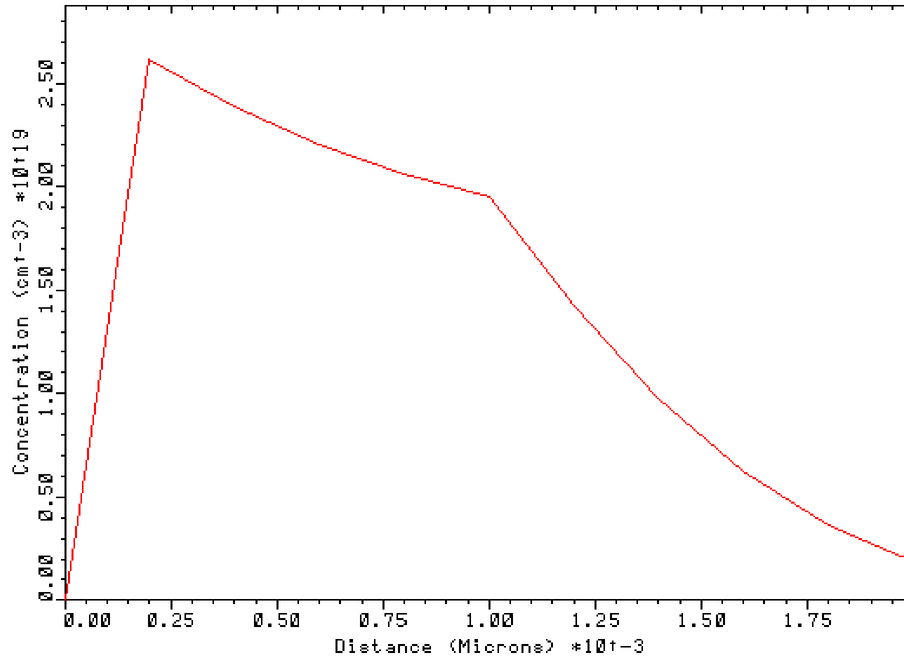

(b)

Figure 2.3: Electron concentration (cm^{-3}) of the channel under the gate-drain access region (a) and gate (b) along the direction perpendicular to device surface for V_{GS}=0 V and V_{DS}=0.05 V. Device surface is assumed to be at x=0.

Figure 2.4 illustrates energy-band diagram before stress under the gate-electrode, along the direction normal to the heterointerface. The inset shows the zoomed-in view of this band diagram at the vicinity of the heterointerface.

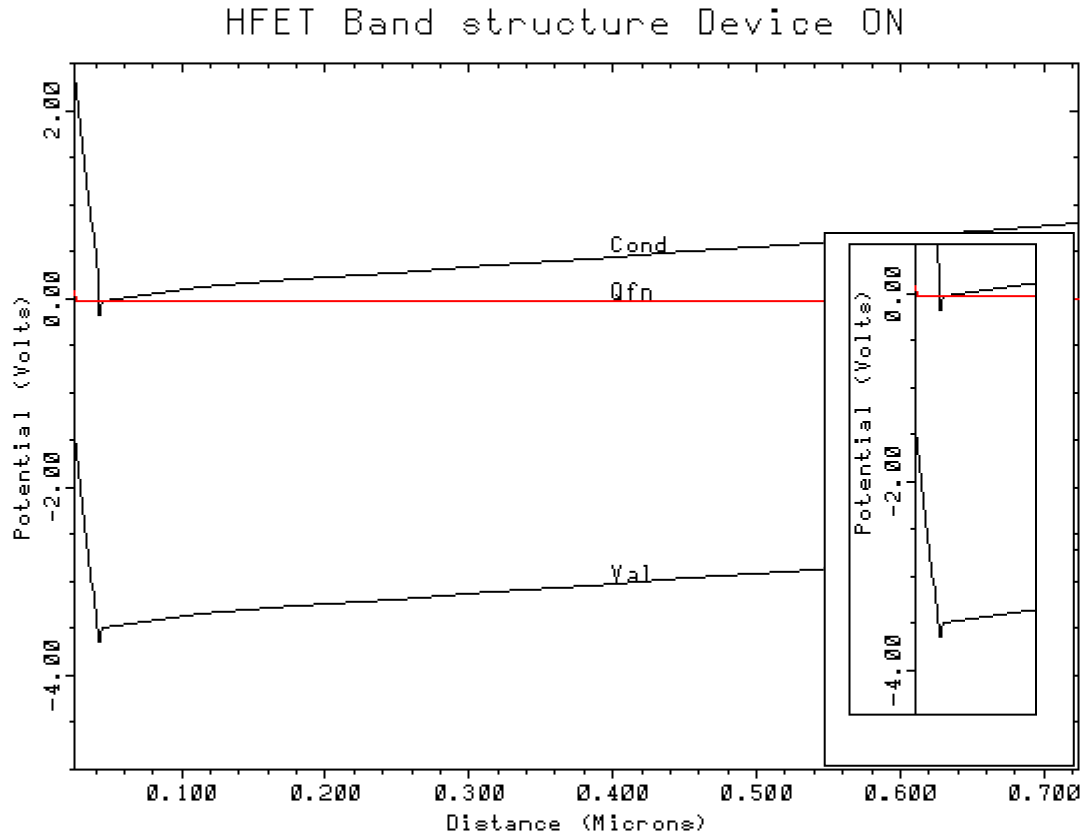

Figure 2.4: Energy-band diagram under the gate along vertical direction for V_{GS}=0 V and V_{DS}=0.05 V. Inset: The zoomed-in view of this energy-band diagram at the vicinity of the heterointerface.

Figure 2.5 illustrates the comparison between the simulation results and an experimental set of drain I/V characteristics for the device before stress. Measurements data are from an AlGaN/GaN HFET grown by molecular beam epitaxy (MBE) on a SiC

substrate [46]. The device had two gate fingers with a gate length of 0.25 μm and a gate finger width of 100 μm. As shown in this figure, a good match is achieved to the experimental values. In the next section, this agreement is used as the basis for the validity of the prediction of surface-charge trapping in substantiation of the post bias-stress characteristics of the same AlGaN/GaN HFET [46].

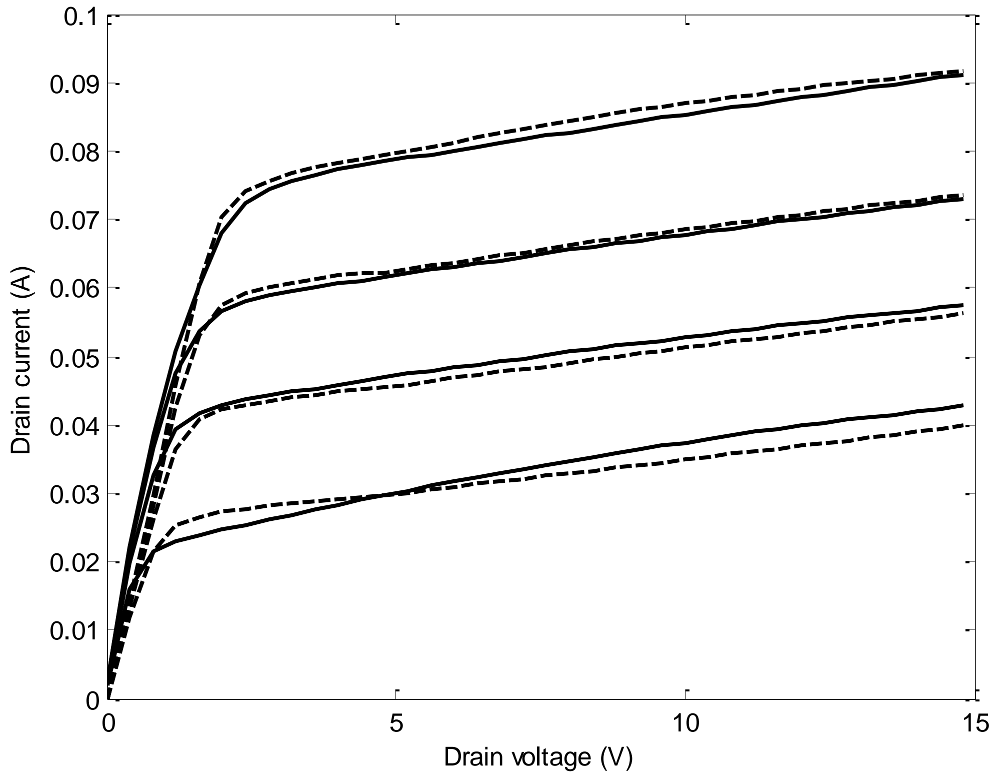

Figure 2.5: I-V characteristics of simulation result (solid line) versus experimental data (dashed line) with the assumption of L_G=0.25 μm and L_{GD}=1.875 μm for V_{GS}=-1.8 V~-3 V with the step of 0.4 V (before stress).

2.2.4.2 After stress

To incorporate the surface charge-trapping effect in the form proposed by Valizadeh *et al.* [46], a thin uniformly doped acceptor-type trap layer has been assumed at the surface of the drain access region. Through trial and error, appropriate values for length,

thickness, doping profile, and interface trap concentration have been chosen to create the best agreement with experimental drain I/V characteristics. This simulation is run by the use of input file 2, which is reported in Appendix B. As it is shown on Figure 2.6, incorporation of this negatively charged surface layer at the gate-side of the drain access region causes the pinching of current flow lines. This can be better seen through comparing the flow lines of this figure to flow lines of this region on Figure 2.2. Figures 2.2 and 2.6 are produced at the same bias point.

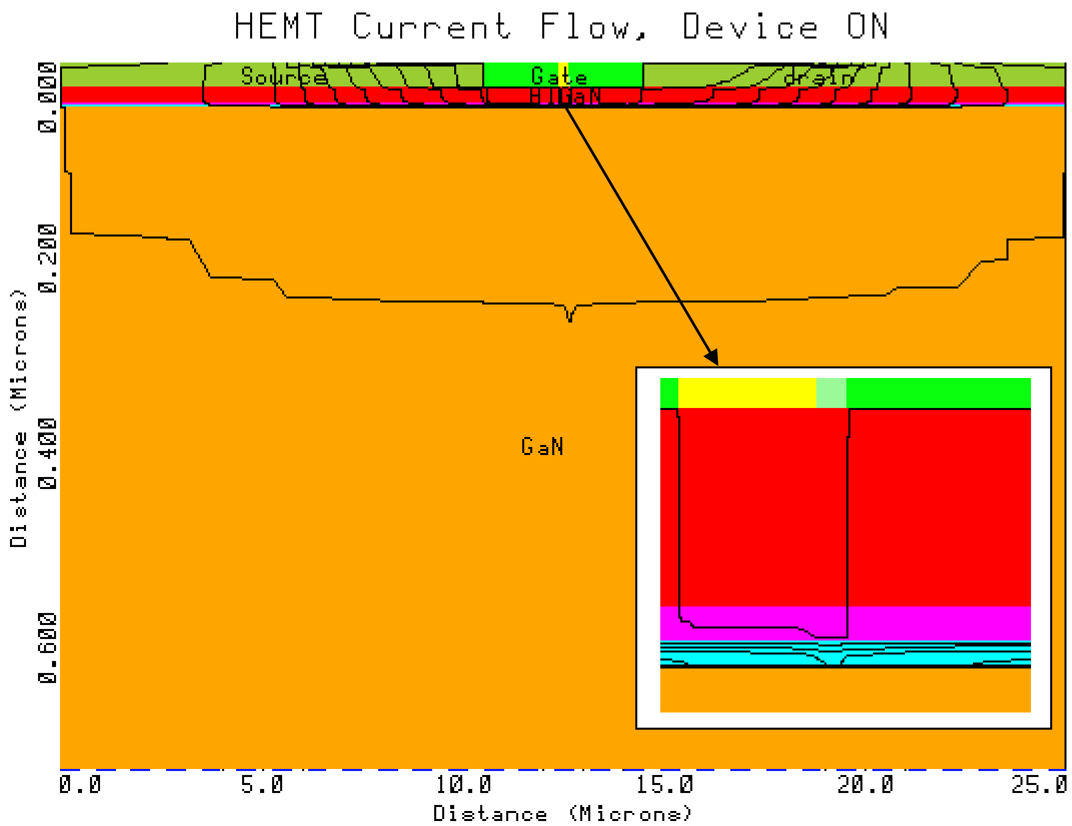

Figure 2.6: Schematic cross section of the presented AlGaN/GaN HFET illustrating current flow after stress for V_{GS}=0 V and V_{DS}=0.05 V.

Figure 2.7 illustrates the electron concentration along the channel for different gate voltages and V_{DS}=5 V. These concentrations are calculated at the peak position of the 2DEG concentration. Results show a significant loss of carrier concentration under

the gate-drain access region. This is due to the incorporation of the negatively charged surface trap layer at the surface of AlGaN barrier in this region. It can be seen that the charge depletion under the gate which was earlier observed on Figure 2.3(c), due to this effect extends towards the drain electrode as the gate voltage approaches the pinch-off voltage. This impact is often reported in terms of the formation of a secondary virtual gate in tandem with the main gate [59].

AlGaN/GaN HFET after stress

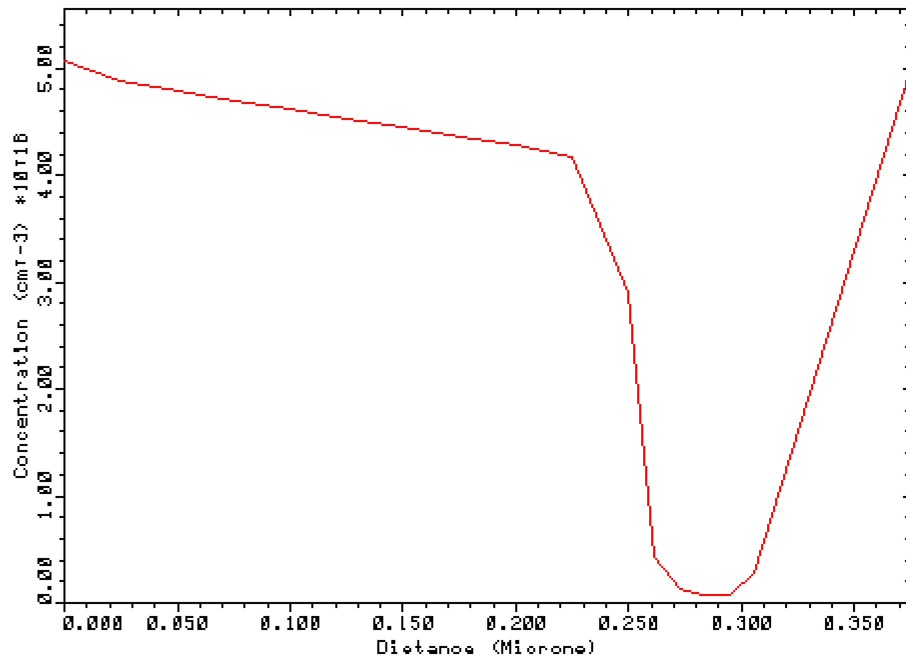

(a)

AlGaN/GaN HFET after stress

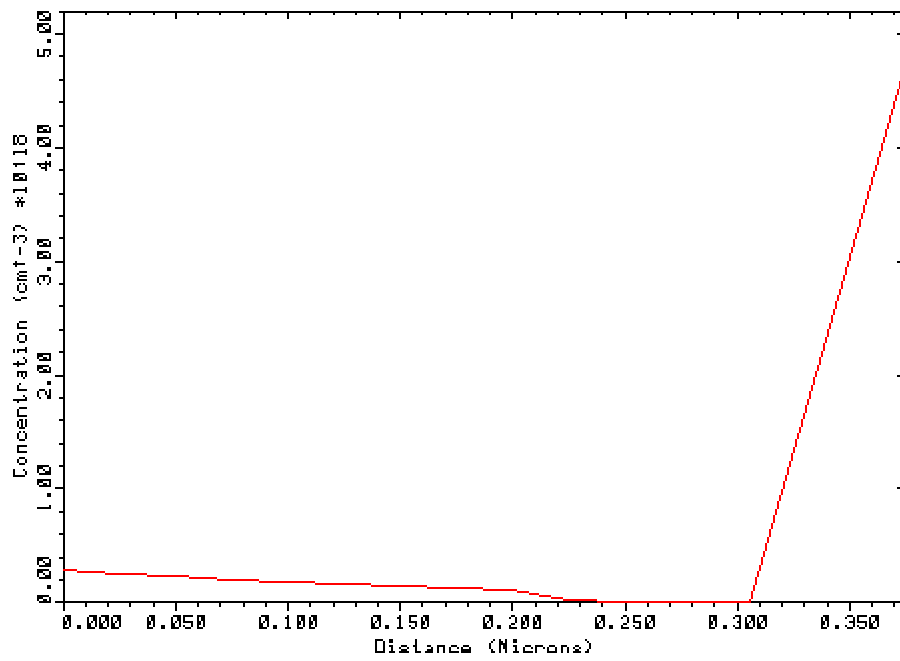

(b)

Figure 2.7: Electron concentration in the channel of the device for V_{GS}=-0.15 V (a) and V_{GS}=-3 V (b) along the longitudinal direction. V_{DS} is equal to 5 V. Source edge of the gate is assumed to be at x=0.

Figure 2.8 illustrates the electric-field along the channel for the device after stress. As is expected the peak electric-field occur at drain edge of the gate.

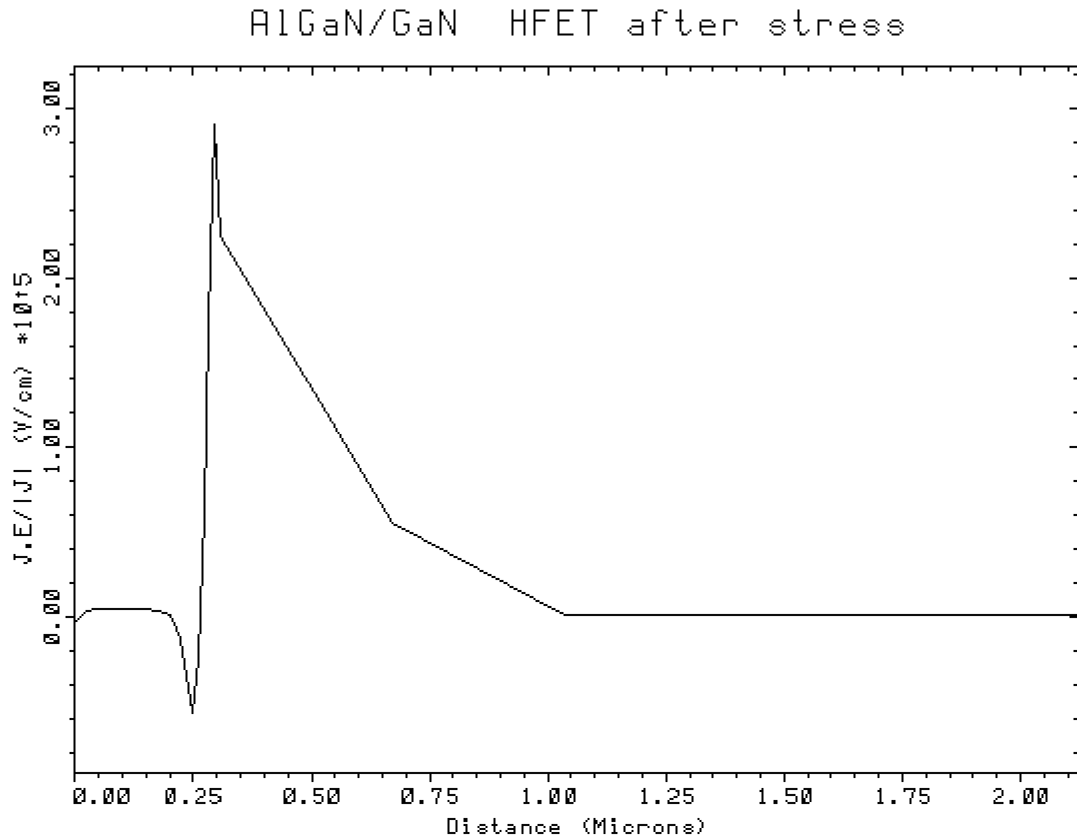

Figure 2.8: Electric-field along the channel after stress for V_{GS}=-1.8 V and V_{DS}=5 V. Source edge of the gate is assumed to be at x=0.

In Figure 2.9, simulation results for I-V characteristic of the device after stress have been compared with experimental data borrowed from [46]. The acceptable agreement between the simulation and experiment validates the speculations of Valizadeh *et al.* [46] on the role of acceptor-type surface traps on drain-current collapse of AlGaN/GaN HFETs.

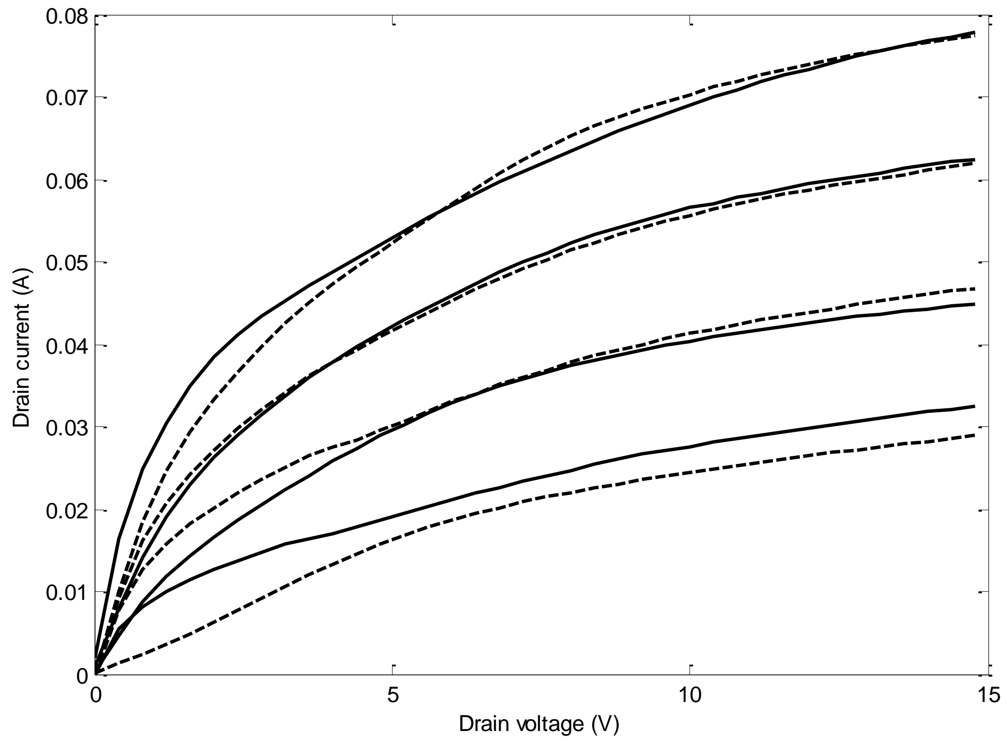

Figure 2.9: I-V characteristics of simulation result (solid line) versus experimental data (dashed line) with the assumption of R_s=0 Ω, R_d=0 Ω, L_G=0.25 μm, and L_{GD}=1.875 μm for V_{GS}=-1.8 V~-3 V with the step of 0.4 V (after stress).

Chapter 3

Analytical Modeling of Drain-Current Characteristics of AlGaN/GaN HFETs with Incorporation of the Impacts of Inflexion Points and Steady-State Velocity Overshoot

3.1 Abstract

An analytical model for drain-current characteristic of AlGaN/GaN HFETs with incorporation of steady-state velocity overshoot and the inflexion points in the electronic drift transport characteristics is presented. Manifestations of these transport characteristics are usually neglected in modeling the drain-current of III-V HFETs. However, significance of these features in AlGaN/GaN material system compared to other III-V technologies requires re-evaluation of this policy. Although for the current

state of the art these features are masked by the parasitic features such as the drain and source contact resistance, by further improvement in the device fabrication technology and reliability of these devices they will deserve further attention. The wide peak and pronounced inflexion points in the transport characteristics of AlGaN/GaN heterojunctions are modeled through considering a drift-diffusion channel rather than a drift-only transport channel. Simulation results have been compared to a non-diffusion type channel implemented with the assumption of Ridley's mobility model. The current model is based on applying an iterative approach between Poisson's equation and current-continuity equation. This relieves the results from the burden of the choice of fitting parameters.

3.2 Introduction

Polar III-Nitride semiconductors, including AlGaN/GaN heterojunction, due to their superb 2DEG concentration, high peak and saturation electron velocity, and wide band-gap have been the target of much attention over the past two decades. With improvements in material growth techniques [60], [61], device fabrication [62], and long-term reliability [63], an increasing need is being felt for development of models that will accurately incorporate particular features of this material system.

The study of Bhapkar *et al.* reveals that in addition to the steady-state velocity overshoot there exists a pronounced kink in the low electric-field region of the drift-velocity versus electric-field characteristics (i.e. $v_d - E$) of GaN [64]. Existence of the inflexion points attributed to this kink and the large width of the overshoot pattern in conjunction with the large electric-fields conventionally applied to this wide band-gap

semiconductor, make the modeling of electronic devices fabricated in this technology different than those of other III-V semiconductors.

In the present work, the influence of the particular $v_d - E$ characteristics of GaN on drain-current characteristic of an AlGaN/GaN HFET is modeled. Presence of these features dictates the formation of consequential electron bunching across the 2DEG channel, especially at high drain voltages. In the present model, variation of electron concentration across the channel is gauged with regards to Poisson's equation and current-continuity equation. The impact of the gradient in electron concentration is modeled by considering the diffusion current component in regions of the channel with electric-field values corresponding to low electric-filed inflexion points and high electric-field negative differential mobility in the $v_d - E$ characteristics.

The degree of complexity of the mobility model employed in a drift-diffusion transport problem is a determinant factor to the possibility of yielding either an analytical or a numerical solution. So far, several mobility models have been proposed or adopted for AlGaN/GaN heterojunctions [65], [66], [67]. Simpler transport models such as Ridley's mobility model [66], which do not incorporate the steady-state velocity overshoot and inflexion points, yield easily solvable analytical models for drain current characteristics of HFETs [68]. However, more elaborate mobility models despite the burden of numerical solutions are worth studying for better projection of the impacts of transport properties on future-generation devices. To incorporate further details of the electronic drift transport of the AlGaN/GaN 2DEG, such as inflexion points in low electric-field region and steady-state velocity overshoot under higher electric-fields, mobility model previously reported by Polyakov *et al.* [67] has been employed in the

present model. Due to the complexity of this mobility model, the analytical model only yields to numerical solutions.

The influence of parasitic contact resistance on drain-current characteristic of an AlGaN/GaN HFET is also investigated. While, an ongoing research effort is pursued by many researchers to improve the Ohmic contact quality of AlGaN/GaN HFETs [69], [70], the current state of the art of this technology still shows masking of transport features in the drain-current characteristics. In this study, the effectiveness of the present model in unveiling these features is revealed. The importance of these considerations is separately gauged for HFETs with self-aligned and non- self-aligned gates.

In section 3.3 details of the implementation of proposed model are presented. In section 3.4 results of the application of this mobility model to the AlGaN/GaN HFETs are presented with respect to the variation of source and drain parasitic contact resistance. These results have been compared to the outcome of the application of the model if Ridley's mobility model was implemented. Conclusions are presented in section 3.5.

3.3 Description of the model

So far, drift transport characteristics of GaN channels, predicted by Monte Carlo simulations [64], [71], [72], [73], to different degrees of approximation have been presented by a few analytical representations [65], [66], [67]. Among these models, Ridley's mobility model provides the most manageable framework for development of an analytical model for drain-current of HFETs [66]. For the current state of the art of this technology, shortcoming of this model in incorporating the steady-state overshoot of

drift-velocity has been deemed acceptable [68]. According to Ridley's drift transport model, electron drift-velocity (i.e. $\nu(E)$) is determined in the form of a two-section model (in which ν_s and E_s are the saturation velocity and electric-field at the onset of velocity saturation and ν_0 is the knee velocity):

$$\nu(E) = \begin{cases} \nu_0 E \dfrac{E + E_1}{E_1(E + E_0)} & E \leq E_s \\ \nu_s & E > E_s \end{cases} \quad \text{where } E_0 = \frac{\nu_0}{\mu_0} \;\; E_1 = \frac{\nu_0}{\mu_1} \tag{3.1}$$

where $\mu_0 = 1000 \dfrac{cm^2}{V.s}, \mu_1 = 50 \dfrac{cm^2}{V.s}, \nu_s = 1.4 \times 10^7 \dfrac{cm}{s}$

Figure 3.1, illustrates the drift-transport characteristics according to this model alongside with the predictions of the mobility model previously investigated by Polyakov *et al.* [67].

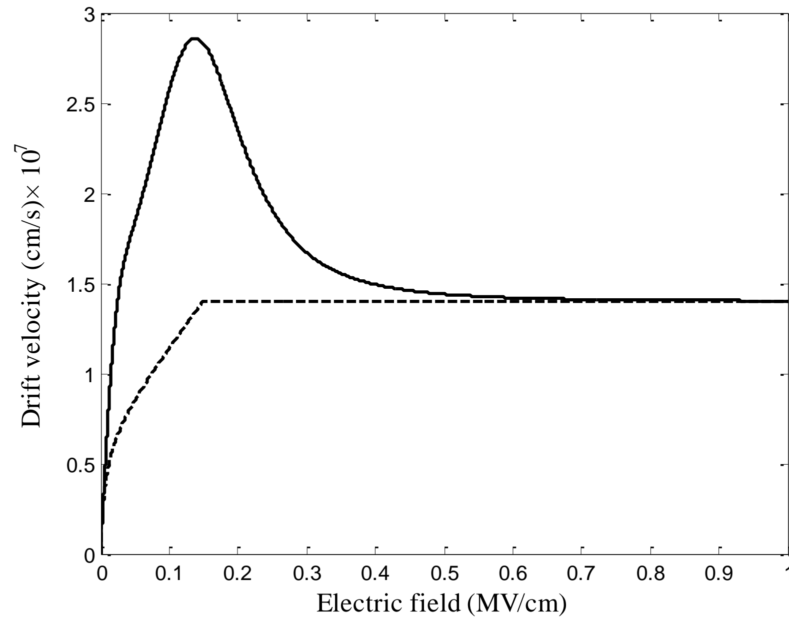

Figure 3.1: Drift-velocity vs. electric-field characteristic of the adopted mobility model (solid line) and Ridley's model (dashed line).

The latter model has been shown to correctly follow the inflexion points and steady-state velocity overshoot patterns envisioned by Monte Carlo simulations for this material system. Drift-velocity according to this mobility model is given by:

$$v(E) = \frac{\mu_0 E + \mu_1 E \left(\frac{E}{E_0}\right)^{\alpha} + v_{sat} \left(\frac{E}{E_1}\right)^{\beta}}{1 + \left(\frac{E}{E_0}\right)^{\alpha} + \left(\frac{E}{E_1}\right)^{\beta}} \tag{3.2}$$

where:

$\mu_0 = 720 \ \frac{cm^2}{Vs}$, $\mu_1 = 234 \ \frac{cm^2}{Vs}$, $E_0 = 3.36 \times 10^4 \frac{V}{cm}$, $E_1 = 9.8 \times 10^4 \frac{V}{cm}$

$\alpha = 2.44, \beta = 7.45$

The parameters of the model have been chosen to provide the maximum similarity to Monte Carol -based predictions of O'Leary *et al.* [73].

In the present work, the $\mathrm{v_d} - \mathrm{E}$ relationship presented by (3.2) has been adopted to engage in studying the impact of the steady-state velocity overshoot and inflexion points observed in Figure 3.1, on drain-current characteristics of AlGaN/GaN HFETs. This investigation has individually targeted devices with self-aligned gates and non- self-aligned gates in subsections 3.3.1 and 3.3.2 of this section, respectively. To extend the breakdown voltage of the device, AlGaN/GaN HFETs, unlike inversion MOSFETs, are traditionally fabricated with non- self-aligned gates. To model an HFET with non- self-aligned gate, the device is broken into an un-gated HFET placed in tandem with an HFET of self-aligned gate. The influence of parasitic contact resistance is also included in this model through incorporation of contact resistance terms of source and drain (i.e. R_S and R_D, respectively). Table 3.1 shows the device parameters used for simulation, unless identified otherwise.

Table 3.1: Parameters used in simulation.

Symbol	DESCRIPTION	Value
R_S	Source contact resistance	5 Ω
R_D	Drain contact resistance	5 Ω
L_{GD}	Gate-drain spacing	1 μm
L_G	Gate length	0.25 μm
W	Device length	200 μm
V_T	Threshold voltage	−3.75 V
d	Barrier thickness	17.5 nm
Δd	2DEG thickness	2 nm
ε_r	$Al_{0.3}Ga_{0.7}N$ relative dielectric constant	8.78

3.3.1 Drain-current simulation of self-aligned HFET

Figure 3.2 schematically shows the cross section of the self-aligned AlGaN/GaN HFET considered in modeling. The approach adopted in modeling the drain-current characteristic of a self-aligned HFET involves splitting of the channel into two regions:

1) Region I is referred to as the linear-region of the channel, along which the electric-field is smaller than the threshold electric-field corresponding to drift-velocity overshoot (i.e. $E_{v\text{-max}}$).

2) Region II is referred to as the saturation-region of the channel, along which the electric-field is beyond $E_{v\text{-max}}$.

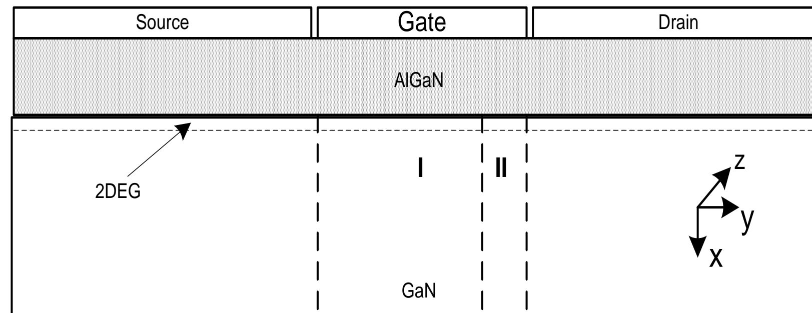

Figure 3.2: Schematic cross-section of a self-aligned AlGaN/GaN HFET. Sections identified by I and II are explained in the text.

Under low drain voltages, as the maximum electric-field is smaller than $E_{\text{v-max}}$, region I will cover the entire length of the channel. With increasing the drain voltage, region II will start to form and expand at the cost of retraction of region I. Regions I and II are treated in sections 3.3.1.1 and 3.3.1.2, respectively.

3.3.1.1 Linear-region characteristics (i.e. $E < E_{\text{v-max}}$)

In this region, by neglecting the gate leakage and leakage through the buffer layer, the drain- current density at any given point along the channel can be written as:

$$J = qn_s(y)v\left(E(y)\right) \tag{3.3}$$

In which, in presence of a gate bias (i.e. V_G), the 2DEG density at the AlGaN/GaN heterointerface can be expressed in terms of threshold voltage V_T:

$$qn_s(y) = C_{ch}\left(V_G - V_T - V(y)\right) \tag{3.4}$$

$V(y)$ is the channel potential and C_{ch} is the gate capacitance per unit area. C_{ch} is calculated by:

$$C_{ch} = \frac{\varepsilon_0 \varepsilon_{AlGaN}}{d + \Delta d} \tag{3.5}$$

where $\varepsilon_{\text{AlGaN}}$ is the relative dielectric constant of the barrier, d is the barrier thickness, and Δd is the effective thickness of the 2DEG, which is typically 2-4 nm for an AlGaN/GaN 2DEG [74].

By substituting (3.2), (3.4), and (3.5) in (3.3), the following relationship between the drain-current density, longitudinal electric-field, and channel potential at any given point in region I will be resulted:

$$\left(1+\left(\frac{E}{E_0}\right)^{\alpha}+\left(\frac{E}{E_1}\right)^{\beta}\right)J=\left(\mu_0.E+\mu_1 E\left(\frac{E}{E_0}\right)^{\alpha}+\nu_{sat}\left(\frac{E}{E_1}\right)^{\beta}\right)C_{ch}\big(V_{GT}-V(y)\big) \quad (3.6)$$

in which V_{GT} is the effective gate voltage. Replacing *E(y)* with the spatial derivative of channel potential in (3.6) leads to the following expression in terms of channel potential (i.e. *V(y)*) and drain-current density (i.e. *J*):

$$\frac{1}{{E_0}^{\alpha}}\left(J-C_{ch}\big(V_{GT}-V(y)\big)\mu_1\frac{dV}{dy}\right)\left(\frac{dV}{dy}\right)^{\alpha}$$

$$+\frac{1}{{E_1}^{\beta}}\left(J-C_{ch}\big(V_{GT}-V(y)\big)v_{sat}\right)\left(\frac{dV}{dy}\right)^{\beta}-C_{ch}\big(V_{GT}-V(y)\big)\mu_0\frac{dV}{dy}+J=0 \qquad (3.7)$$

Equation (3.7) requires numerical solution and can be solved by using the finite difference technique. To obtain the characteristics between the drain-current density and channel potential at the end of region I, for each gate voltage, *J* is swept from zero to 1 A/mm in very small increments. Continuity of the electric-field along the channel, current continuity in the drift-only channel, and boundary condition of the grounded source electrode are applied in this solution. In solving this equation longitudinal electric-field should be monitored. This equation is valid as long as this electric-field is smaller than $E_{\text{v-max}}$. The channel potential recorded at the end of region I (i.e. $V_{\text{D-v-max}}$), is imported to section 3.3.1.2 for each value of gate voltage.

3.3.1.2 Saturation-region characteristics (i.e. E>$E_{\text{v-max}}$)

Early reduction of carrier drift-velocity in region II and later saturation of drift-velocity (depending on the maximum value of drain voltage) in conjunction with current continuity dictate the materialization of electron bunching in this part of the channel.

Consequences of this phenomenon on the carrier drift characteristics of FETs have been considered on all the viable models presented for these devices after the seminal work of Grebene *et al.* [75]. These models have been based on silicon-like purely saturating $v_d - E$ characteristics. While the model of Grebene *et al.* purely addresses this phenomenon through incorporation of the impact of the vertical electric-field in this region, in the current work presence of the steady state drift-velocity overshoot and creation of non-zero gradient in carrier concentration also demand the incorporation of a diffusion current term in region II.

According to the model of Grebene *et al.*, to incorporate the impact of electron bunching in region II, Gauss's law has been applied to the rectangular Gaussian box shown in Figure 3.3.

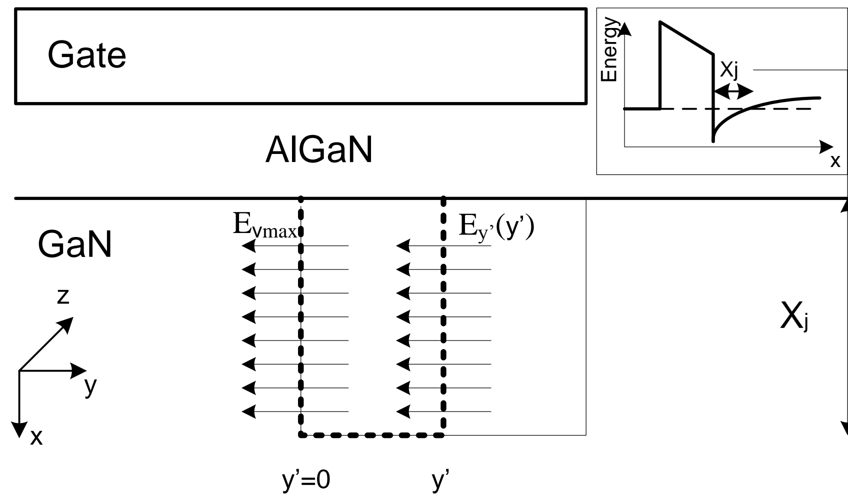

Figure 3.3: Schematic cross-section of a self-aligned AlGaN/GaN HFET, illustrating the Gaussian box used in the analysis of saturation-region. The inset shows the conduction band-edge at the AlGaN/GaN heterointerface.

This box fully extends throughout region II. In this figure, X_j marks the depletion layer thickness in GaN which is unintentionally doped to N_{GaN}. According to this:

$$\oint \vec{E}.\overrightarrow{dS} = \frac{Q_{tot}}{\varepsilon_s} \tag{3.8}$$

where E is the electric-field, $\overrightarrow{ds}$ is the surface element, and Q_{tot} is the total charge enclosed by the Gaussian box. The absence of a Z-directed electric-field reduces (3.8) to a two dimensional equation:

$$-\left(\int_0^{y'} \frac{Q_n(y")}{\varepsilon_{GaN}} dy" + \frac{qN_{GaN}X_j}{\varepsilon_{GaN}} y'\right) = -E_y\,(y')X_j + E_{v-max}\,X_j - \frac{\varepsilon_{AlGaN}}{\varepsilon_{GaN}} \int_0^{y'} E_{\perp}(0, y")\,dy" \tag{3.9}$$

Here, X_{j} is assumed to be large enough so that the normal electric-filed on the bottom surface of the Gaussian box is negligible. The normal electric-field to AlGaN/GaN heterointerface (i.e. $E_{\perp}$) is given by:

$$E_{\perp}(0, y') = \frac{1}{d + \Delta d}\left(V_{GT} + \frac{Q_B}{C_{ch}} - V(y')\right) \tag{3.10}$$

where Q_{B} is the total bulk charge in GaN region enclosed by the Gaussian box.

Q_{n} in (3.9) is the sheet charge density and unlike the assumption of Grebene *et al.* for the mobility model of the current work (i.e. (3.2)) it is not assumed to be constant:

$$Q_n(y') \simeq C_{ch}\left(V_{GT}{}' - V(y')\right) \tag{3.11}$$

In this form, the position dependency of the sheet charge density along the length of region II is incorporated through the variation of channel potential (i.e. $V(y')$) and the threshold voltage $V_{\text{T}}{}'(y')$, which has been taken into account in $V_{\text{GT}}{}'$ which is defined as $V_{\text{G}} - V_{\text{T}}'(y')$. In the model of Grebene *et al.* the constant profile of sheet charge density

has been maintained by assuming the same position dependency for the threshold voltage and channel potential. Although this is correct for a saturating $\mathrm{v_d} - \mathrm{E}$ profile, it will not be acceptable for the mobility model of (3.2). As it is explained later in this section, the profile of threshold voltage will be calculated through iteratively solving (3.9) with the current-continuity equation.

By inserting (3.10) and (3.11) in (3.9), the following relationship between the device threshold voltage (i.e. V_{T}) and the effective-threshold voltage of region II (i.e. $V'_{\mathrm{T}}(y')$) is achieved:

$$X_j \frac{\partial E(y')}{\partial y'} = -\frac{C_{ch}}{\varepsilon_{GaN}}(V_T - V'_T(y')) \tag{3.12}$$

In solving for the position dependency of the threshold voltage in region II, the channel-potential and electric-field distributions of [75] can be taken as initial assumptions:

$$E(y') = E_{v-max} cosh\left(\frac{y'}{\lambda}\right) \tag{3.13}$$

$$V(y') = V_{D-v-max} + \lambda E_{v-max}\ sinh\left(\frac{y'}{\lambda}\right) \tag{3.14}$$

In which, $V_{\mathrm{D-v-max}}$ is the channel potential at the end of region I and has been imported from the calculations performed in that region. In this work, initial value of the parameter λ is taken equal to 30 nm which is in the range of values reported in literature for modeling the behavior of AlGaN/GaN HFETs [68]. Adoption of these initial profiles to (3.12) will result in an initial guess for $V'_{\mathrm{T}}(y')$ which according to (3.11) will result in a position dependent profile for $Q_{\mathrm{n}}(y')$. Variation in sheet charge density in region II is

then used for calculating the diffusion current component in this region. After this step, the assumption of the drift-only channel which was inherited from (3.3) should be revisited by deducting the position dependent diffusion current density at any given point along the channel in region II from the total value of the drain-current density (i.e. J). This correction for achieving a revised profile for $V_T'(y')$ is described below:

$$J_{drift} = J - J_{diff} \tag{3.15}$$

$$V_T'(y') = V_G - V(y') - \frac{J_{drift}(y')}{C_{ch}\, v(y')} \tag{3.16}$$

Plugging this new profile of effective threshold voltage in (3.12) will result in revised profiles for the channel-potential and electric-field along the length of region II. Continuity of electric-field should be maintained at the boundary of regions I and II. For every value of gate-voltage (i.e. V_G) and drain-current (i.e. J) this procedure is repeated until convergence. For iterative solution and convergence visual examination was used. The aforementioned correction of the drift current component is applicable to that portion of region II in which $E(y')$ is smaller than the velocity-saturation electric-field. Beyond this point, assumption of Grebene *et al.* in the form of (3.13) and (3.14) will be valid. The values of λ and $V_{D\text{-}v\text{-}max}$ should be appropriately chosen to maintain continuity of electric-field to the point immediately located before this point in the channel. This procedure is illustrated in Figure 3.4.

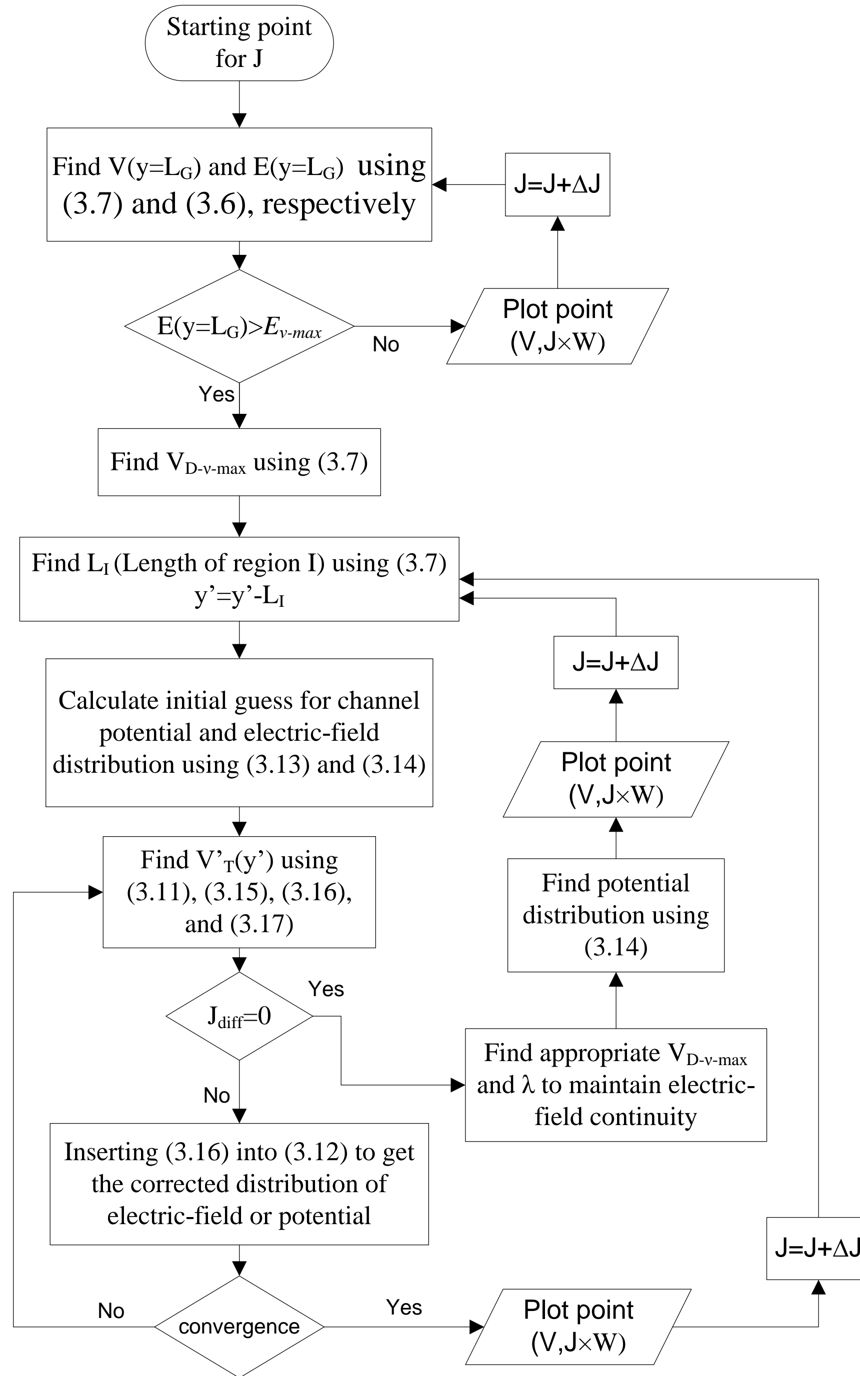

Figure 3.4: Simulation flowchart for the self-aligned AlGaN/GaN HFET.

Diffusion component of current is calculated by using following expression:

$$J_{diff}(y') = \frac{k_B T}{q} \frac{v(y')}{E(y')} \frac{dQ_n(y')}{dy'} \tag{3.17}$$

where, k_B is the Boltzmann constant, T is the temperature in Kelvin and q is the charge of an electron. In this expression the simple form of Einstein's relationship for a non-degenerate semiconductor is employed. Later in section 3.4, it is demonstrated that despite the fact that this form is not fully applicable to a degenerate 2DEG, the impact of the full incorporation of Einstein relationship will be negligible.

3.3.2 Drain-current simulation of non- self-aligned HFET

Figure 3.5 schematically shows the cross section of the simulated non- self-aligned AlGaN/GaN HFET. As it is apparent from this figure, this device can be envisioned as the tandem connection of a self-aligned HFET with an un-gated HFET.

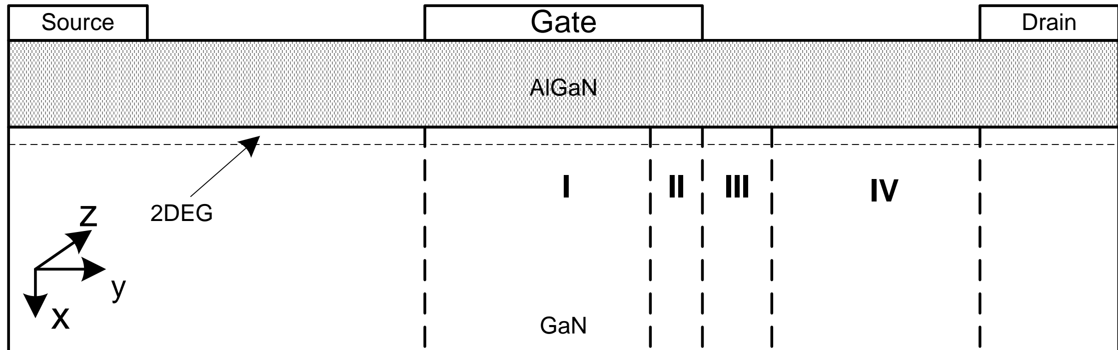

Figure 3.5: Schematic cross-section of a non- self-aligned AlGaN/GaN HFET. Sections identified by I, II, III and IV are explained in the text.

The approach adopted in the present model for a non- self-aligned HFET is based on splitting of the channel into four regions: linear region (region I) and saturation region (region II) of the gated HFET, and saturation region (region III) and linear region (region

IV) of the un-gated HFET. In this analogy, form of the profile of the electric-field in the drain-access region of a FET requires the charge carrier of the un-gated HFET to be considered of opposite polarity. As a result, the role of source and drain is reversed in the un-gated HFET.

While the relationship between the current and voltage at the drain edge of gate for each value of gate voltage can be calculated according to the procedure explained in section 3.3.1, the potential drop across the drain access-region is accounted for by implementing a procedure very close to that of Figure 3.4 on this un-gated HFET. The only difference in this implementation is that in this region in the absence of a metallic gate, a surface potential term should instead be considered. In support of this argument, it should be reminded that the theory of metal semiconductor junction, due to lack of consideration of surface states, has the tendency to overestimate the role of metal work function. In this implementation, the current continuity and continuity of electric-field between regions II and III is maintained. In absence of an actual gate voltage, the role of the apparent spatial variation of the surface potential can be lumped into the variation of threshold voltage. This is a valid strategy as in the calculation of charge concentration along the channel the difference between $V_{\mathrm{G}}(y')$ and $V_{\mathrm{T}}'(y')$ and not their individual values is of interest. The value of the constant part of surface potential (used in place of V_G in equations of section 3.3.1) is set by swiping V_{G} and finding the proper value for which the electric-field continuity is maintained at the boundary of regions II and III.

3.4 Simulation results and discussions

Figure 3.6 illustrates an example of convergence of threshold voltage, diffusion current density, and electric-field in saturation region of the channel (i.e. region II). Acceptable levels of convergence after 6 steps of iteration have been observed to reduce the burden of choosing the fitting parameter (i.e. λ).

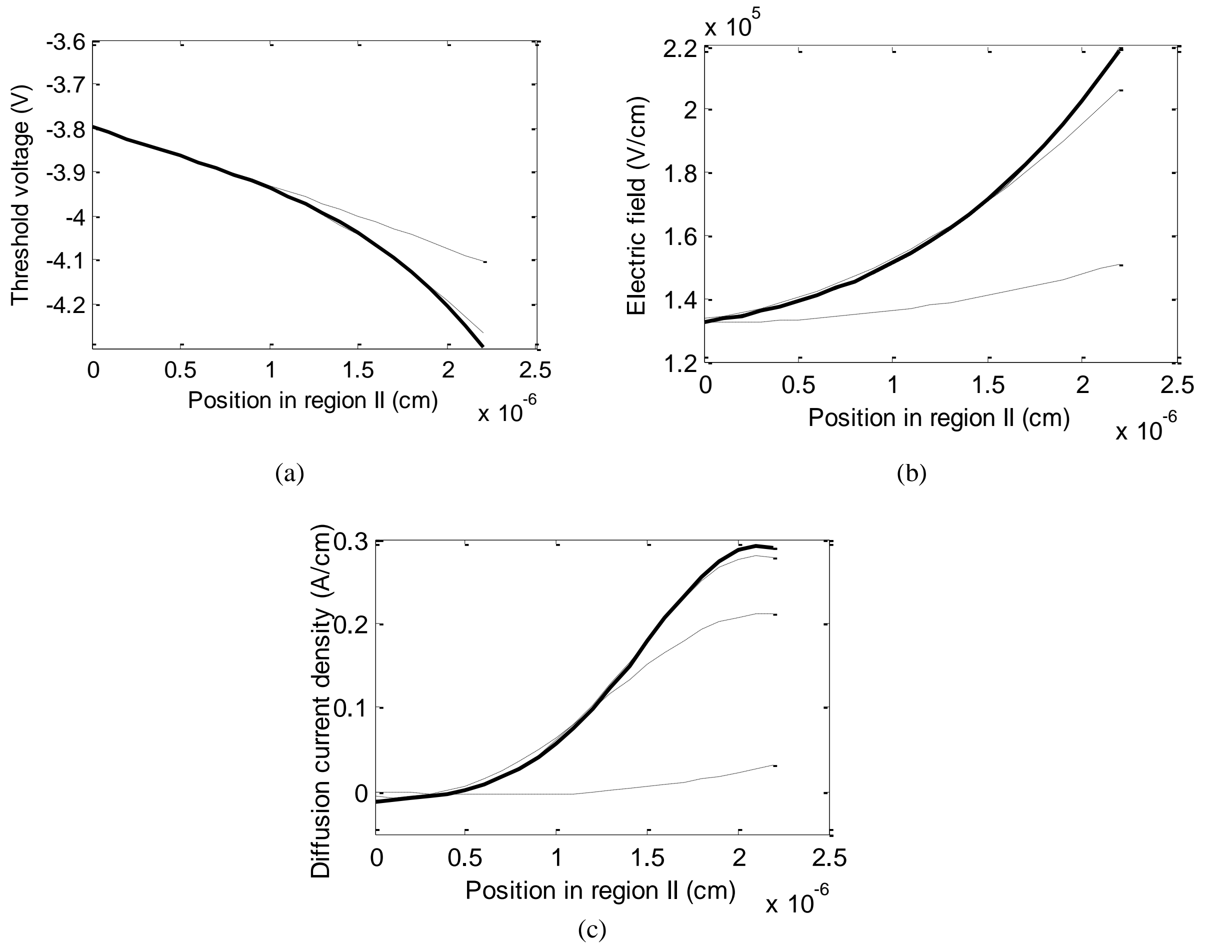

Figure 3.6: Convergence of threshold voltage distribution (a), electric-field distribution (b), and diffusion current density (c) in region II after 6 steps of iteration for V_{GS}=-1.8 V, I=124 mA. Convergence is achieved to the curve shown in solid line. R_S and R_D are equal to 5 Ω.

Figure 3.7(a) and (b) illustrate two sets of calculated drain-current versus drain-source voltage characteristics of a self-aligned and a non- self-aligned AlGaN/GaN

HFET for gate-source voltages of -1.8, -2.2, -2.6, and -3 V, respectively. Two different mobility models have been used in the implementation of the proposed model. Continuous curves show the result of adoption of (3.2) while broken curves are representative of adoption of Ridley's saturating mobility model (i.e. (3.1)).

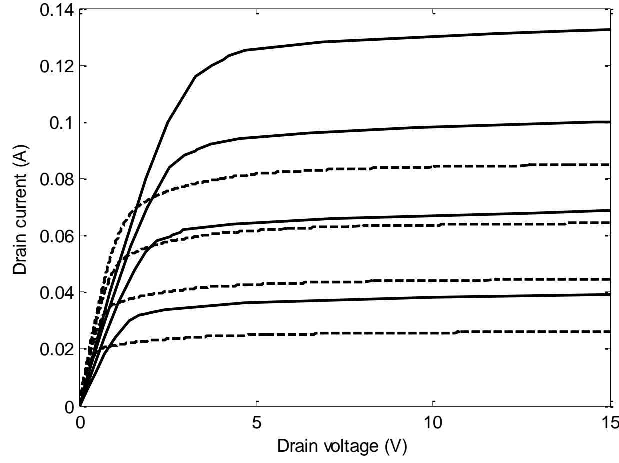

(a)

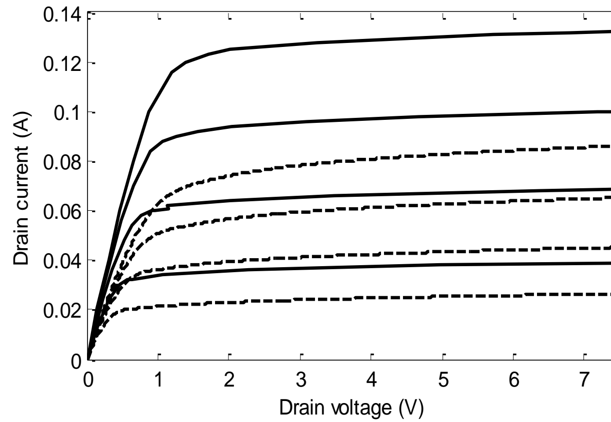

(b)

Figure 3.7: Drain I-V characteristics based on mobility model of (3.2) (solid curve) versus Ridley's mobility model (dashed curve) for V_{GS}=-1.8~-3.0 V with steps of 0.4 V for a non-self-aligned HFET (a) and a self-aligned HFET (b). R_S and R_D are equal to 5 Ω.

On Figures 3.8, 3.9, and 3.10, these data are presented for drain/source contact resistance of 0, 20, and 35 Ω, respectively. Due to higher drift-velocity at the low electric-field region predicted by (3.2), which is illustrated in Figure 3.1, the drain-current

calculated for this model is higher than the predictions of Ridley's mobility model. As it is demonstrated in Figures 3.8-3.10, by increasing the contact resistance the two sets of data will further mimic one another, especially at higher drain voltage. This observation is valid for both the self-aligned and non- self-aligned HFETs. This is due to the masking effect of the parasitic contact resistance on features such as inflexion points and steady state velocity overshoot that are present in the mobility model of (3.2).

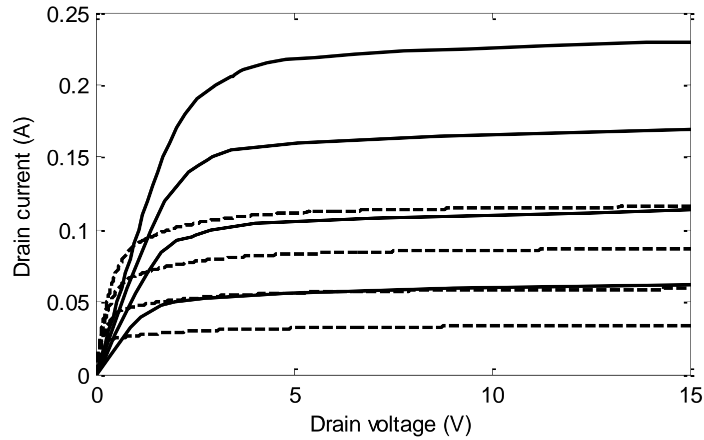

(a)

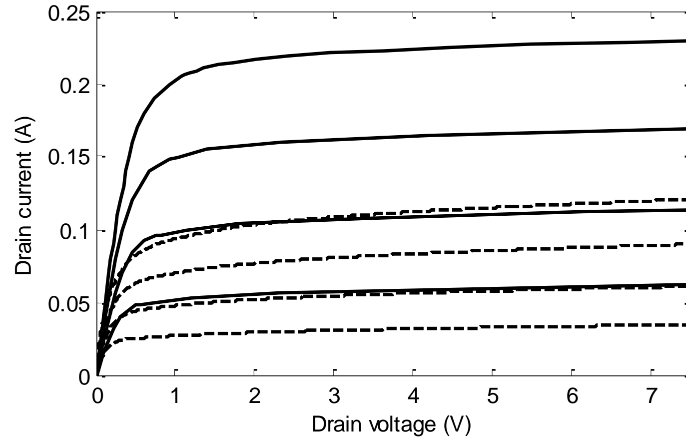

(b)

Figure 3.8: Drain I-V characteristics based on mobility model of (3.2) (solid curve) versus Ridley's mobility model (dashed curve) for V_{GS}=-1.8~-3.0 V with steps of 0.4 V for a non-self-aligned HFET (a) and a self-aligned HFET (b). R_S and R_D are equal to 0 Ω.

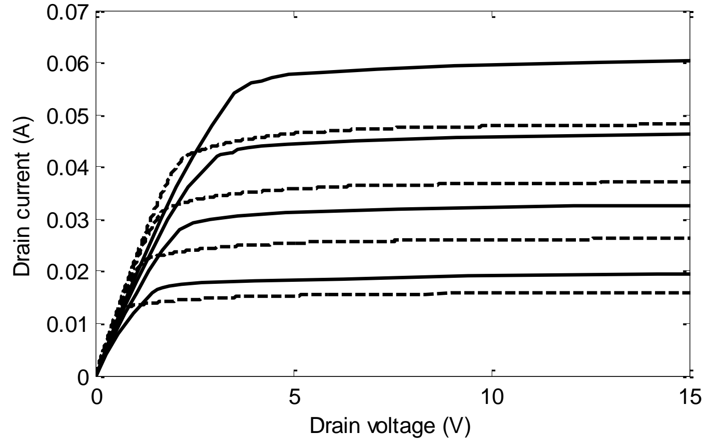

(a)

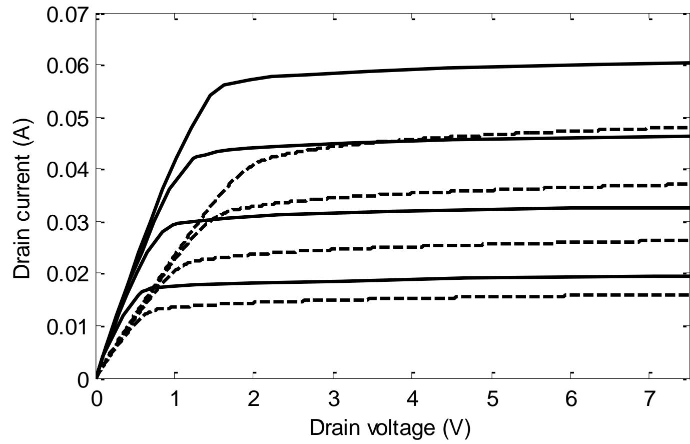

(b)

Figure 3.9: Drain I-V characteristics based on mobility model of (3.2) (solid curve) versus Ridley's mobility model (dashed curve) for V_{GS}=-1.8~-3.0 V with steps of 0.4 V for a non-self-aligned HFET (a) and a self-aligned HFET (b). R_S and R_D are equal to 20 Ω.

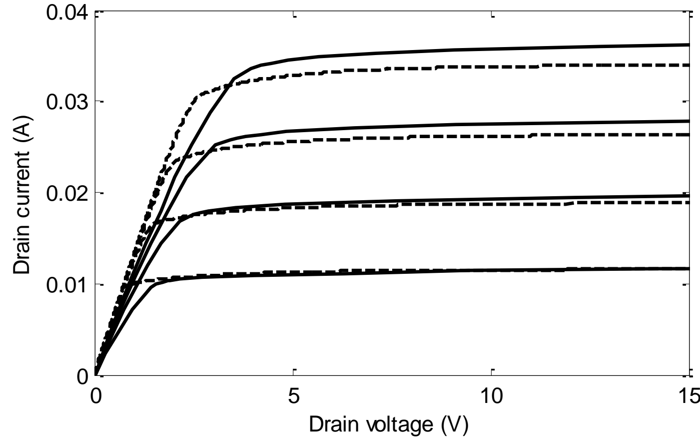

(a)

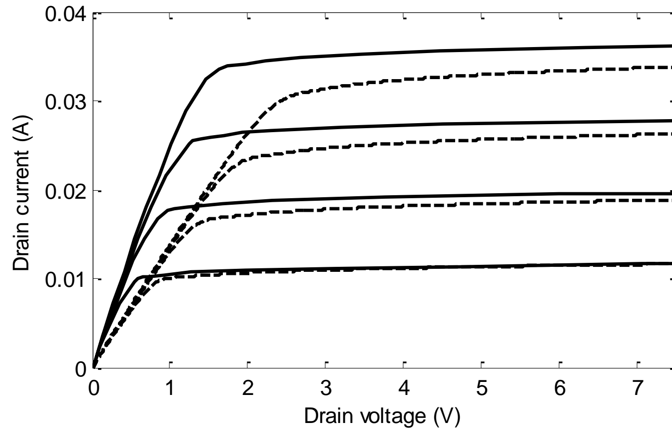

(b)

Figure 3.10: Drain I-V characteristics based on mobility model of (3.2) (solid curve) versus Ridley's mobility model (dashed curve) for V_{GS}=-1.8~-3.0 V with steps of 0.4 V for a non-self-aligned HFET (a) and a self-aligned HFET (b). R_S and R_D are equal to 35 Ω.

Figure 3.11 demonstrates the matching between the calculated drain I-V characteristics based on Ridley mobility model (with assumption of drain-source contact resistance of 5 Ω) and borrowed measurement results from an AlGaN/GaN HFET [46]. Measurements have been performed on an AlGaN/GaN HFET grown by molecular beam epitaxy (MBE) on a SiC substrate. The device has two gate fingers with a gate length of 0.25 μm and a gate finger width of 100 μm. The closely-matched characteristics are indicative of high value of contact resistance of the measured devices. These observations indicate that contrary to the traditional assumptions of negligible impact of steady-state

velocity overshoot on drain-current characteristics of III-V HFETs, for AlGaN/GaN HFETs the exact nature of the drift-transport can have very substantial impacts on the drain-current among other characteristics. This is due to the broader overshoot pattern and also larger value of electric-field normally applied to these wide band-gap HFETs.

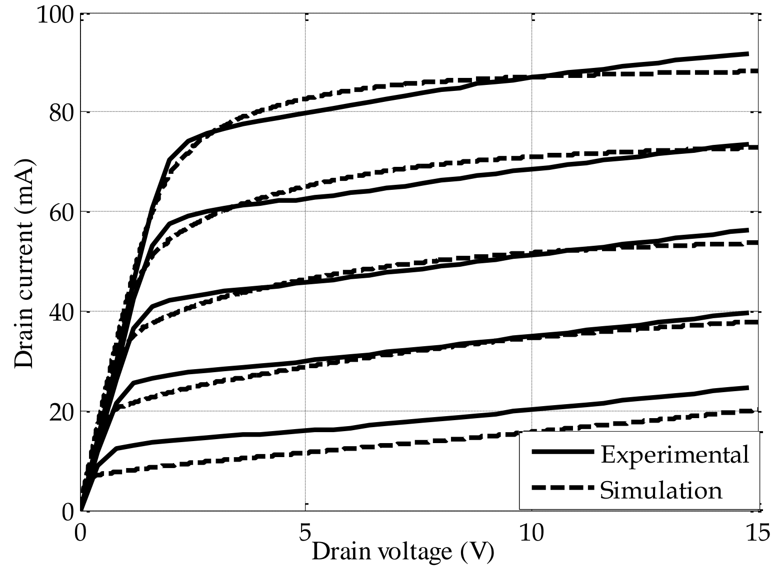

Figure 3.11: Drain I-V characteristics based on Ridley's mobility model (solid curve) versus experimental measurements (dashed curve) for V_{GS}=-1.8~-3.4 V with steps of 0.4 V. The simulated device is a non-self-aligned HFET with R_S and R_D of 5 Ω, and L_{GD}=1.875 μm. The mismatch close to threshold voltage is due to the lack of consideration of leakage through buffer layer.

Despite the fact that these features are masked by parasitic effects such as contact resistance in the current state of technology, with the constant technological improvement of III-Nitride HFETs [70], [76], a more complete inclusion of transport characteristics in the fashion presented in this thesis, becomes a necessity.

The degeneracy of the 2DEG has been neglected in (3.17). In order to more accurately study the impact of the degenerated channel on drain-current characteristic of AlGaN/GaN HFETs, the maximum correction factor (based on the maximum carrier kinetic energy in the channel) in the full form of Einstein relationship has been

calculated. As the worst case scenario, neglecting the position dependency of this correction factor, Figure 3.12 illustrates the results with respect to incorporation of this correction factor in (3.17). The inset of Figure 3.12 shows the variation of the correction factor versus the reduced Fermi level [77]. Due to negligible difference between the results with and without incorporation of this correction factor, the implementation of the presented model based on the simple form of Einstein relationship is deemed sufficient.

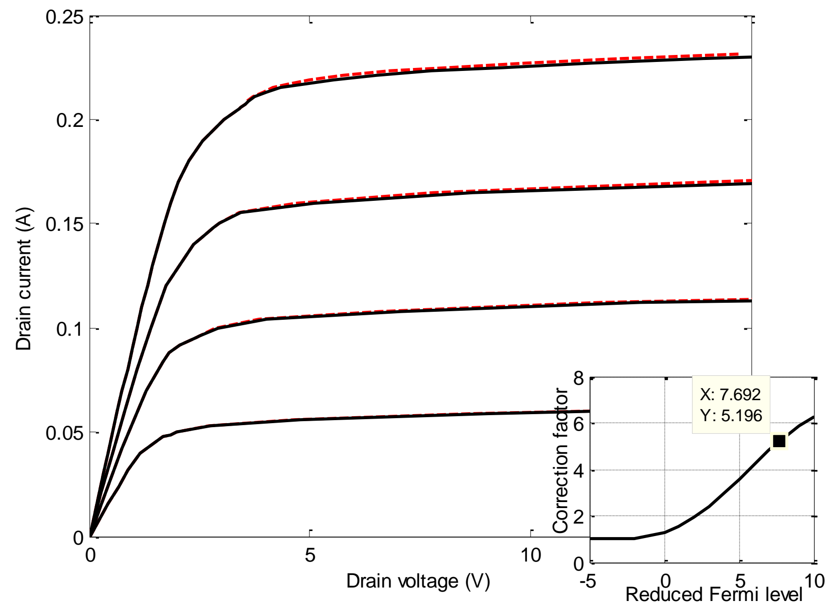

Figure 3.12: Drain I-V characteristics based on simple Einstein's relationship (solid line) versus corrected Einstein's relationship (dashed line) for a non-self-aligned HFET with the assumption of $R_S=R_D=0\ \Omega$, $L_G=0.25\ \mu m$, and $L_{GD}=1.0\ \mu m$ for V_{GS}=-1.8V~-3.0V with the step of 0.4 V. Inset: Correction factor as a function of reduced Fermi level $\eta=\frac{E_F-E_C}{K_BT}$.

In order to demonstrate the importance of inclusion of inflexion points of the $v_d - E$ characteristics of AlGaN/GaN channel, impacts of these features via comparing the outcomes of the proposed model versus the result of adoption of a mobility model incapable of representing the inflexion points are studied. Figure 3.13, shows the $v_d - E$ characteristics according to the model earlier presented by Shey *et al.* [65]. This model is presented as:

$$v(x) = \frac{\mu_0 E(x) + v_s \left(\frac{E(x)}{E_1}\right)^5}{1 + \left(\frac{E(x)}{E_0}\right)^5} \tag{3.18}$$

Constant of this model, have been chosen as a best match to Monte Carlo predictions of O'Leary *et al.* [73]. These constants have been reported as [78]:

$\mu_0 = 260 \left({cm^2}/{V.s}\right)$, $v_s = 2.10 \times 10^7\ ({cm}/{s})$,

$E_0 = 15.9 \times 10^4\ \left({V}/{cm}\right)$, $E_1 = 17.2 \times 10^4\ \left({V}/{cm}\right)$

This model has been used for studying the drain I/V characteristics of non- self-aligned AlGaN/GaN HFETs with parameters indicated in Table 3.1, unless identified otherwise.

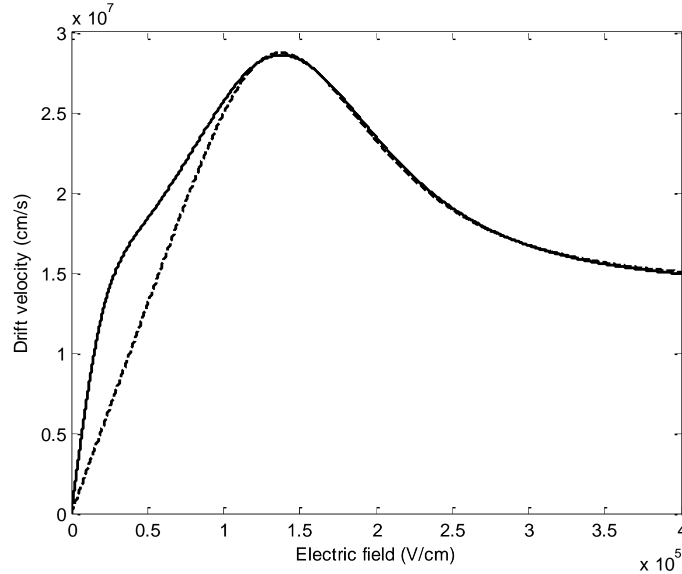

Figure 3.13: v_d-E characteristics according to (3.2) and (3.18).

Figure 3.14, illustrates the result of the adoption of this mobility model to the model presented in section 3.3.2, versus the outcome of that model based on mobility

model of (3.2). On Figure 3.14(a), (b), and (c) the gate length has been taken as 0.25 μm, 0.5 μm, and 1 μm, respectively. All other parameters of these devices are the identical.

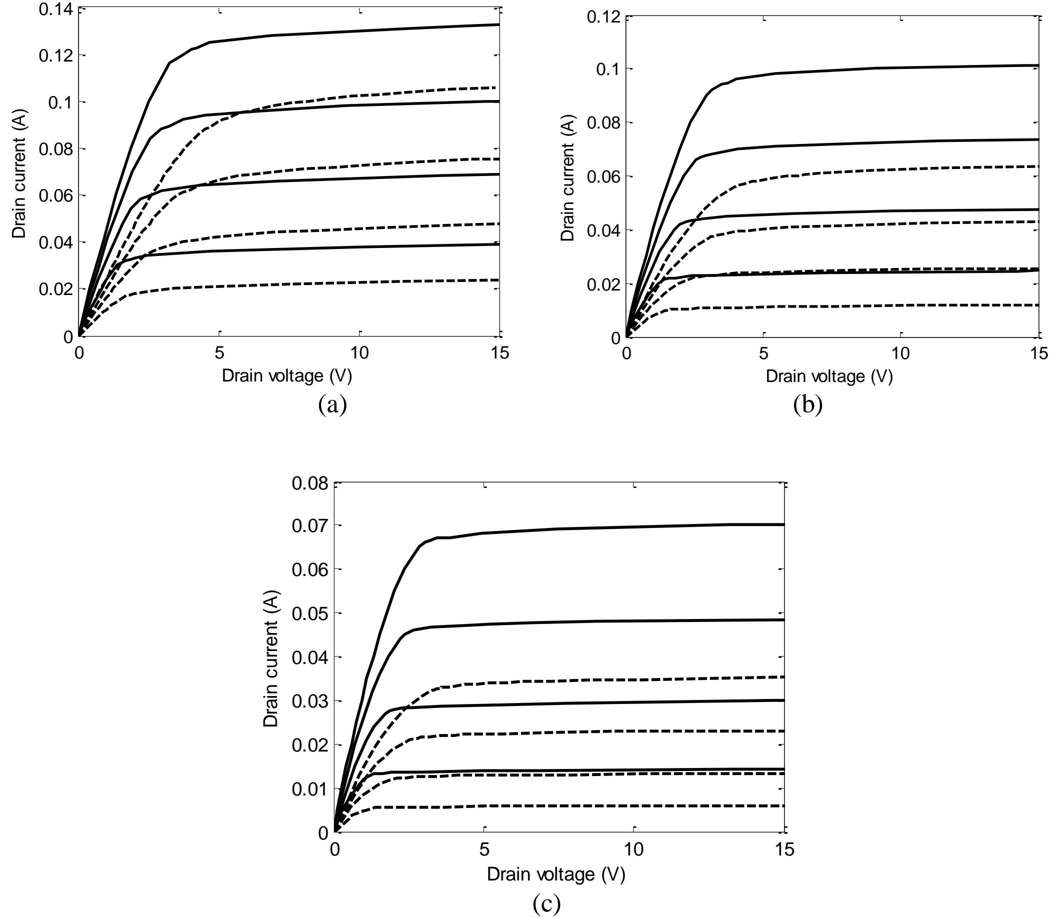

Figure 3.14: Drain I-V characteristics based on mobility model of (3.2) (solid line), versus (3.18) (dashed line) for L_G=0.25 μm (a), L_G=0.5 μm (b), and L_G=1 μm (c), for V_{GS}=-1.8~-3.0 V with steps of 0.4 V.

Figure 3.15, illustrates the result of the adoption of mobility model of (3.18) to the model presented in section 3.3.2, versus the outcome of that model based on mobility model of (3.2). On Figure 3.15(a), (b), and (c) the gate-drain spacing has been taken as 1 μm, 2 μm, and 3 μm, respectively. All other parameters of these devices are the identical.

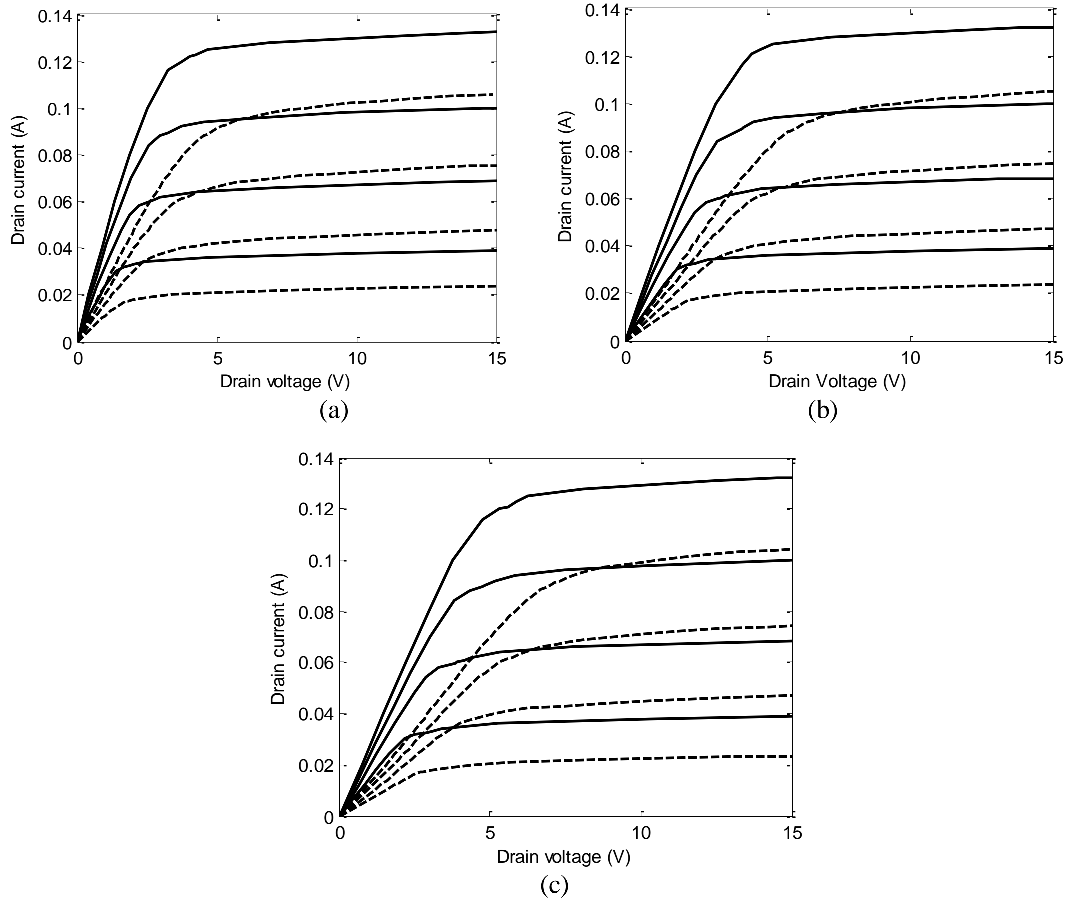

Figure 3.15: Drain I-V characteristics based on mobility model of (3.2) (solid line), versus (3.18) (dashed line) for L_{GD}=1 μm (a), L_{GD}=2 μm (b), and L_{GD}=3 μm (c), for V_{GS}=-1.8~-3.0 V with steps of 0.4 V.

As it is observed on Figure 3.14 and Figure 3.15, the similarity between the outcomes of the two mobility models grows as the gate-length and gate-drain spacing are reduced. This is due to the fact that for short channel devices, under a proportionally longer part of the channel carriers are exposed to higher electric-fields for which the two models, as presented in Figure 3.13, predict identical drift velocities. This argument can be applied both to gated and the ungated HFETs of Figure 3.5.

3.5 Conclusion

An analytical model for drain-current characteristic of AlGaN/GaN HFETs with incorporation of inflexion points and steady-state velocity overshoot is proposed. The application of this model to HFETs, with and without self-aligned gates, reveals the tangible impact of these features on drain-current characteristics of HFETs. The presented model, which is based on iterative solution of current-continuity and Poisson's equations, is quite independent of the choice of fitting parameters. It is shown that by technological improvement of the Ohmic contacts in III-Nitride technology, the effects of transport features such as inflexion points and steady-state velocity overshoot gains further relevance in producing highly reliable models for these devices. It has been observed that the inflexion points of drift transport characteristics will play a more prominent role in the drain characteristics of devices of longer gate length and gate-drain spacing. This is specially highlighted by the improvement in quality of Ohmic contacts to AlGaN/GaN heterojunctions.

Chapter 4

Conclusion and Future Works

4.1 Goals and contributions of the thesis

This thesis had the main goal of modeling the drain-current characteristic of AlGaN/GaN HFETs with incorporation of electron trapping at deep surface states and detailed drift transport characteristics. To demonstrate the validity of the models, results have been compared with experimental data.

4.2 Conclusions

Current collapse and reliability degradation due to electron trapping at the surface layer of AlGaN/GaN HFETs are the major concerns in this technology. Current collapse suppresses microwave output power performance of the device. Even though considerable improvements have been made in this technology trapping effects in AlGaN/GaN HFETs have not been removed.

In chapter 2, an assured simulation of AlGaN/GaN HFET including trapping effects was presented using CADtool Medici®. The simulation has been performed for

the device before stress and after stress and the results have been compared with experimental observation of Valizadeh *et al*. [46]. After stress results show a significant loss of carrier concentration under the gate-drain access region which is due to the incorporation of the negatively charged surface trap layer at the surface of AlGaN barrier in this region. The acceptable agreement between the simulation and experimental data validates the speculations of Valizadeh *et al.* [46] on the role of acceptor-type surface traps on drain-current collapse of AlGaN/GaN HFETs.

In chapter 3, an analytical model for drain-current characteristic of AlGaN/GaN HFETs with incorporation of inflexion points and steady-state velocity overshoot is proposed. The application of this model to AlGaN/GaN, with and without self-aligned gates, reveals the significant impact of these features on drain-current characteristics of AlGaN/GaN HFETs. The model is quite independent of the choice of fitting parameters due to iterative nature of this approach. It is shown that by technological improvement of the Ohmic contacts in III-Nitride technology, the effects of transport features such as inflexion points and steady-state velocity overshoot gains further relevance in producing highly reliable models for these devices. It has been observed that the inflexion points of drift transport characteristics will play a more prominent role in the drain characteristics of devices of longer gate length and gate-drain spacing. This is specially highlighted by the improvement in quality of Ohmic contacts to AlGaN/GaN heterojunctions.

4.3 Future works

This research concludes with specific direction to future work. Extension of the present model to accommodate the impacts of gate leakage and leakage through substrate is

suggested as a viable future direction. Also it is suggested that implementing a more accurate charge trapping profile at AlGaN layer with incorporation of the impact of the traps in other locations of the device such as barrier and buffer layer will improve the matching between experimental data and simulation results. Study of the time constant of these trapping/de-trapping mechanisms in regards to the energy-level, emission rate, and capture cross-section of the traps can cast light on the frequency response of these processes.

In addition, incorporating the thermal effects which were completely absent from the current studies on the drain-current characteristic of AlGaN/GaN HFETs is deemed as a very important future direction for this work.

Bibliography

[1] M. Khan, Q. Chen, J. Yang, M. Anwar, M. Blasinggame, M. Shur, J. Burm, and L. Eastman, "Recent advances in III-V nitride electron devices," *IEDM Technical Digest*, pp. 27-30, Dec. 1996.

[2] R. Trew, "Wide bandgap semiconductor transistors for microwave power amplifiers," *IEEE Microwave Magazine,* vol. 1, no. 1, pp. 46-54, Mar. 2000.

[3] J. Wu, W. Walukiewiewica, K. Yu, J. Ager, E. Hakker, H. LU, W. Schaff, Y. Saito, and Y. Nanishi, "Unusual properties of the fundamental band gap of InN," *Applied Physics Letters*, vol. 80, no. 21, pp. 3967-3969, May 2002.

[4] http://www.ioffe.rssi.ru/SVA/NSM/Semicond/InN/bandstr.html#Basic or M. Levinshtein, S. Rumyantsev, and M. Shur, Properties of advance semiconductor materials, J. Wiley and sons, 2001.

[5] C. Monier, F. Ren, J. Han, P. Chang, R. Shul, K. Lee, A. Zhang, A. Baca, and S. Pearton, "Simulation of npn and pnp AlGaN/GaN heterojunction bipolar transistors performances: limiting factors and optimum design," *IEEE Transactions on Electron Devices,* vol. 48, no. 3, pp. 427-432, Mar. 2001.

[6] O. Ambacher, J. Smart, J. Shealy, N. Weimann, K. Chu, M. Murphy, W. Schaff, L. Eastman, R. Dimitrov, L. Wittmer, M. Stutzmann, W. Rieger, and J. Hilsenbeck, "Two-dimensional electron gases induced by spontaneous and piezoelectric polarization charges in N- and Ga-face AlGaN/GaN heterostructures," *Journal of Applied Physics*, vol. 85, no. 6, pp. 3222-3233, Mar. 1999.

[7] K. Takahashi, A. Yoshikawa, and A. Sandhu, Wide bandgap semiconductors: fundamental properties and modern photonic and electronic devices, Springer, 2007.

[8] T. Mimura, "The Early History of the High Electron Mobility Transistor (HEMT)," *IEEE Transactions on Microwave Theory and Techniques*, vol. 50, no. 3, pp. 780-782, Mar. 2002.

[9] F. Schwierz and J. Liou, "Semiconductor devices for RF applications: evolution and current status," *Microelectronic Reliability.*, vol. 41, no. 2, pp. 145-168, Feb. 2001.

[10] M. S. Shur, "GaN based transistors for high power applications," *Journal of Solid-State Electronics*, vol. 42, no. 12, pp. 2131-2138, Dec. 1998.

[11] U. Mishra and J. Singh, Semiconductor device physics and design, Springer, 2008.

[12] M. Khan, J. Kuznia, D. Olson, W. Schaff, J. Burm, and M. Shur, “Microwave performance of a 0.25 µm gate AlGaN/GaN heterostructure field effect transistor,” *Applied Physics Letters*, vol. 65, no. 9, pp. 1121–1123, Aug. 1994.

[13] H. Morkoç, Handbook of Nitride Semiconductors and Devices, vol. 1: Materials Properties, Physics and Growth, Weinheim: Wiley, 2009.

[14] E. Yu and E. Manasreh, “Spontaneous and piezoelectric polarization in nitride heterostructures,” in III-V Nitride Semiconductors: Applications and Devices (Optoelectronic Properties of Semiconductors and Superlattices), pp. 161-193, Taylor & Francis, 2003.

[15] http://www.cree.com, News bulletin of Cree Inc.

[16] U. Mishra, P. Parikh, and Y. Wu, “AlGaN/GaN HEMT an overview of device operation and application,” *Proceedings of the IEEE*, vol. 90, no 6, pp. 1022-1031, June 2002.

[17] R. Vetury, N. Zhang, S. Keller, and U. Mishra, “The impact of surface states on the DC and RF characteristics of AlGaN/GaN HFETs,” *IEEE Transactions on Electron Devices*, vol. 48, no. 3, pp. 560–566, Mar. 2001.

[18] P. Valizadeh and D. Pavlidis, “Low Frequency Noise-based Monitoring of the Effects of RF and DC Stress on AlGaN/GaN MODFETs,” *proceedings of GaAs IC Symposium*, pp. 78-81, Nov. 2003.

[19] W. Lu, V. Kumar, R. Schwindt, E. Piner, and I. Adesida, “A comparative study of surface passivation on AlGaN/GaN HEMTs,” *Journal of Solid-State Electronics*, vol. 46, no.9, pp. 1441-1444, Sep. 2002.

[20] B. Green, K. Chu, E. Chumbes, J. Smart, J. Shealy, and L. Eastman, “The effect of surface passivation on the microwave characteristics of undoped AlGaN/GaN HEMTs,” *IEEE Electron Device Letters*, vol. 21, no. 6, pp. 268-270, June 2000.

[21] T. Maffeis, M. Simmonds, S. Clark, F. Peiro, P. Haines, and P. Parbrook, “Near ideal, high barrier, Au-nGaN Schottky contacts,” *Journal of Physics D: Applied Physics*, vol. 33, no. 20, pp. 115-118, Oct. 2000.

[22] L. Eastman, V. Tilak, J. Smart, B. Green, E. Chumbes, R. Dimitrov, H. Kim, O. Ambacher, N. Weimann, T. Prunty, M. Murphy, W. Schaff, and J. Shealy, “Undoped AlGaN/GaN HEMTs for microwave power amplification,” *IEEE Transactions on Electron Devices*, vol. 48, no. 3, pp. 479-485, Mar. 2001.

[23] S. Keller, Y. Wu, G. Parish, N. Zhang, J. Xu, B. Keller, S. DenBaars, and U. Mishra, “Gallium nitride based high power heterojunction field effect transistors: process development and present status at UCSB,” *IEEE Transactions on Electron Devices*, vol. 48, no. 3, pp. 552-559, Mar. 2001.

[24] M. Higashiwaki, N. Onojima, T. Matsui, and T. Mimura, “Effects of SiN passivation by catalytic chemical vapour deposition on electrical properties of AlGaN/GaN heterostructure field-effect transistors,” *Journal of Applied Physics*, vol. 100, no. 3, pp. 0337141-0337146, Aug. 2006.

[25] W. Tan, P. Houston, P. Parbrook, G. Hill, and R. Airey, “Comparison of different surface passivation dielectrics in AlGaN/GaN heterostructure field-effect transistors,” *Journal of Physics D: Applied Physics*, vol. 35, no. 7, pp. 595–598, Apr. 2002.

[26] N. Tsurumi, H. Ueno, T. Murata, H. Ishida, Y. Uemoto, T. Ueda, K. Inoue, and T. Tanaka, “AlN Passivation Over AlGaN/GaN HFETs for Surface Heat Spreading,” *IEEE Transactions on Electron Devices*, vol. 57, no. 5, pp. 980-985, May 2010.

[27] A. Griffin, F. Brotzen, and P. Loos, “The effective transverse thermal conductivity of amorphous Si_3N_4 thin films,” *Journal of Applied Physics*, vol. 76, no. 7, pp. 4007–4011, Oct. 1994.

[28] G. Slack, R. Tanzilli, R. Pohl, and J. Vandersande, “The intrinsic thermal conductivity of AlN,” *Journal of Physics and Chemistry of Solids*, vol. 48, no. 7, pp. 641–647, 1987.

[29] S. Karmalkar, D. Sathaiya, and M. Shur, “Mechanism of the reverse gate leakage in AlGaN/GaN high electron mobility transistors,” *Applied Physics Letters*, vol. 82, no. 22, pp. 3976–3978, June 2003.

[30] S. Karmalkar, D. Sathaiya, “On the resolution of the mechanism for reverse gate leakage in AlGaN/GaN HEMTs,” *IEEE Electron device letters,* vol. 27, no. 2, pp. 87-89, Feb. 2006.

[31] E. Miller, X. Dang, and E. Yu, “Gate leakage current mechanisms in AlGaN/GaN heterostructure field-effect transistors,” *Journal of Applied Physics*, vol. 88, no. 10, pp. 5951-5958, Nov. 2000.

[32] J. Spradlin, S. Dogan, M. Mikkelson, D. Huang, L. He, D. Johnstone, H. Morkoç, and R. Molnar, “Improvement of n-GaN Schottky diode rectifying characteristics using KOH etching,” *Applied Physics Letters*, vol. 82, no. 20, pp. 3556-3558, May 2003.

[33] I. Grzegory, B. Lucznik, M. Bockowski, and S. Porowski “Crystallization of low dislocation density GaN by high-pressure solution and HVPE methods,” *Journal of Crystal Growth*, vol. 300, no. 1, pp. 17-25, March 207.

[34] F. Lipski, T. Wunderer, S. Schwaiger, and F. Scholz, “Fabrication of freestanding 2 "-GaN wafers by hydride vapour phase epitaxy and self-separation during cooldown ,” *8th International Conference on Nitride Semiconductors*, pp. 1287-1291, Oct. 2009.

[35] Y. Oshimura, K.Takeda, T. Sugiyama, M. Iwaya, S. Kamiyama, H. Amano, I. Akasaki, A. Bandoh, and T. Udagawa, "AlGaN/GaN HFETs on Fe-doped GaN substrates," *Physics Status Solidi (c)*, vol. 7, no. 7–8, pp. 1974–1976, July 2010.

[36] P. Boguslawski, E. Briggs, and J. Bernholc, "Native defects in gallium nitride," *Physical Review B*, vol. 51, no. 23, pp. 17255–17258, June 1995.

[37] X. Ning, F. Chien, P. Pirouz, J. Yang, and M. Khan, "Growth defects in GaN films on sapphire: The probable origin of threading dislocations," *Journal of Materials Research*, vol. 11, no. 3, pp. 580-592, Mar. 1996.

[38] www.eudyna.com, News bulletin of Sumitomo Electronics Device Innovations Inc.

[39] www.nitronex.com, News bulletin of Nitronex Corporation.

[40] www.rfmd.com, News bulletin of RFMD Inc.

[41] www.kymatech.com, News bulletin of Kyma Technologies Inc.

[42] G. Meneghesso, G. Verzellesi, R. Pierobon, F. Rampazzo, A. Chini, U. Mishra, C. Canali, and E. Zanoni, "Surface-related drain current dispersion effects in AlGaN–GaN HEMTs," *IEEE Transactions on Electron Devices*, vol. 51, no. 10, pp. 1554-1561, Oct. 2004.

[43] M. Khan, M. Shur, Q. Chen, and J. Kuznia, "Current/voltage characteristic collapse in AlGaN/GaN heterostructure insulated gate field effect transistors at high drain bias," *Electronics Letters,* vol. 30, no. 25, pp. 2175–2176, Dec. 1994.

[44] S. Bradley, A. Young, L. Brillson, M. Murphy, W. Schaff, and L. Eastman, "Influence of AlGaN deep level defects on AlGaN/GaN 2DEG carrier confinement," *IEEE Transactions on Electron Devices*, vol. 48, no. 3, pp. 412–415, Mar. 2001.

[45] A. Koudymov, G. Simin, M. Khan, A. Tarakji, R. Gaska, and M. Shur, "Dynamic current-voltage characteristics of III-N HFETs," *IEEE Electron Device Letters*, vol. 24, no. 11, pp. 680-682, Nov. 2003.

[46] P. Valizadeh and D. Pavlidis, "Effects of RF and DC Stress on AlGaN/GaN MODFETs: A Low-Frequency Noise-Based Investigation," *IEEE Transactions on Device and Materials Reliability*, vol. 5, no. 3, pp. 555-563, Sep. 2005.

[47] S. Binari, P. Klein, and E. Kazior, "Trapping Effects in GaN and SiC Microwave FETs," *Proceedings of the IEEE*, vol. 90, no. 6, pp. 1048-1058, June 2002.

[48] S. Binari, K. Ikossi, J. Roussos, W. Kruppa, D. Park, H. Dietrich, D. Koleske, A. Wickenden, and R. Henry, "Trapping effects and microwave power performance in

AlGaN/GaN HEMTs," *IEEE Transactions on Electron Devices*, vol. 48, no. 3, pp. 465-471, Mar. 2001.

[49] P. Klein, S. Binari, J. Freitas, and A. Wickenden, "Photoionization spectroscopy of traps in GaN metal-semiconductor field-effect transistors," *Journal of Applied Physics*, vol. 88, no. 5, pp. 2843-2852, Sep. 2000.

[50] P. Valizadeh and D. Pavlidis "Investigation of the impact of Al mole-fraction on the consequences of RF stress on $Al_xGa_{1-x}N$/GaN MODFETs," *IEEE Transactions on Electron Devices*, vol. 52, no. 9, pp. 1933-1939, Aug. 2005.

[51] B. Green, V. Kaper, V. Tilak, J. Shealy, and L. Eastman, "Dynamic loadline analysis Of AlGaN/GaN HEMTS," *Proceedings of IEEE Lester Eastman Conference on high performance devices*, pp. 443-452, Aug. 2002.

[52] Medici manual, Synopsis Inc., Mountain view, CA.

[53] O. Ambacher, B. Foutz, J. Smart, J. Shealy, N. Weimann, K. Chu, M. Murphy, A. Sierakowski, W. Schaff, L. Eastman, R. Dimitrov, A. Mitchell, and M. Stutzmann, "Two dimensional electron gases induced by spontaneous and piezoelectric polarization in undoped and doped AlGaN/GaN heterostructures," *Journal of Applied Physics*, vol. 87, no. 1, pp. 334-344, Jan. 2000.

[54] P. Valizadeh, E. Alekseev, D. Pavlidis, F. Yun, and H. Morkoç¸ "Anomalous effects of temperature and UV illumination on the operation of AlGaN/GaN MODFET," *Journal of Solid-State Electronics*, vol. 50, no.2, pp. 282-286, Feb. 2006.

[55] P. Valizadeh, "High-temperature very low frequency noise-based investigation of slow transients in AlGaN/GaN MODFETs," *IEEE Transactions on Device and Materials Reliability*, vol. 8, no. 2, pp. 265-271, June 2008.

[56] S. Datta, Quantum transport: Atom to transistor, Cambridge University Press, 2005.

[57] S. Karmalkar and U. Mishra, "Enhancement of breakdown voltage in AlGaN/GaN high electron mobility transistors using a field plate," *IEEE Transactions on Electron Devices*, vol. 48, no. 8, pp. 1515-1521, Aug. 2001.

[58] T. Anderson, M. Tadjer, M. Mastro, J. Hite, K. Hobart, C. Eddy, and F. Kub, "Demonstration of Enhancement Mode AlN/ultrathin AlGaN/GaN HEMTs Using A Selective Wet Etch Approach," *Proceedings of Compound Semiconductor Manufacturing Technology*, pp. 197-199 , 2010.

[59] M. Moradi and P. Valizadeh, "Analytical Modeling of Current Collapse in AlGaN/GaN HFETs According to the Virtual Gate Concept," *IEEE Transactions on Device and Materials Reliability*, vol. 10, no. 2, pp. 287-294, June 2010.

[60] K. Fujito, S. Kubo, and I. Fujimura, "Development of bulk GaN crystals and nonpolar/semipolar substrates by HVPE," *MRS Bulletin,* vol. 34, no. 5, pp. 313-317, Apr. 2009.

[61] R. Dwilinski, R. Doradzinski, J. Garczynski, L.P. Sierzputowski, A. Puchalski, Y. Kanbara, K. Yagi, H. Minakuchi, and H. Hayashi, "Bulk ammonothermal GaN," *Journal of Crystal Growth*, vol. 311, no. 10, pp. 3015-3018, May 2009.

[62] H. Lin, H. Yu, and F. Huang, "Performance improvement of AlGaN/GaN HEMTs using two-step silicon nitride passivation," *Microwave and Optical Technology Letters*, vol. 52, no. 7, pp. 1614-1619, July 2010.

[63] E. Heller, "Simulation of life testing procedures for estimating long-term degradation and lifetime of AlGaN/GaN HEMTs," *IEEE Transactions on Electron Devices*, vol. 55, no. 10, pp. 2554-2560, Oct. 2008.

[64] U. Bhapkar and M. Shur, "Monte Carlo calculation of velocity-field characteristics of wurtzite GaN," *Journal of Applied Physics*, vol. 82, no. 4, pp. 1649-1655, May 1997.

[65] A. Shey and W. Ku, "An analytical current-voltage characteristics model for high electron mobility transistors based on nonlinear charge-control formulation," *IEEE Transactions on Electron Devices*, vol. 36, no. 10, pp. 2299-2306, Oct. 1989.

[66] B. Ridley, "Coupled surface and channel transport in semiconductor heterostructures," *Journal of Applied Physics*, vol. 90, no. 12, pp. 6135–6139, Dec. 2001.

[67] V. Polyakov and F. Schwierz, "Influence of electron mobility modeling on DC I–V characteristics of WZ-GaN MESFETs," *IEEE Transactions on Electron Devices*, vol. 48, no. 3, pp. 512–516, Mar. 2001.

[68] A. Koudymov, M. Shur, G. Simin, K. Chu, P. Chao, C. Lee, J. Jimenez, and A. Balistreri, "Analytical HFET I-V model in presence of current collapse," *IEEE Transactions on Electron Devices*, vol. 55, no. 3, pp. 712-720, Mar. 2008.

[69] Q. Feng, L. Li, Y. Hao, J. Ni, and J. Zhang "The improvement of ohmic contact of Ti/Al/Ni/Au to AlGaN/GaN HEMT by multi-step annealing method," *Journal of Solid-State Electronics,* vol. 53, no. 9, pp. 955-958, Sep. 2009.

[70] F. Mohammed, L. Wang, H. Koo, and I. Adesida, "Anatomy-performance correlation in Ti-based contact metallizations on AlGaN/GaN heterostructures," *Journal of Applied Physics,* vol. 101, no. 3, pp. 033708.1-033708.15, Feb. 2007.

[71] J. Kolnik, I. Oguzman, K. Brennan, R. Wang, P. Ruden, and Y. Wang, "Electron transport studies of bulk zinc blende and wurtzite phases of GaN based on ensemble

Monte Carlo calculation including a full zone band structure," *Journal of Applied Physics*, vol. 78, no. 2, pp. 1033-1038, July 1995.

[72] J. Albrecht, R. Wang, P. Ruden, M. Farahmand, and K. Brennan, "Electron transport characteristics of GaN for high temperature device modeling," *Journal of Applied Physics*, vol. 83, no. 9, pp. 4777-4781, May 1998.

[73] S. O'Leary, B. Foutz, M. Shur, and L. Eastman, "Steady-state and transient electron transport within the III–V nitride semiconductors, GaN, AlN, and InN: a review", *Journal of Materials Science: Materials in Electronics*, vol. 17, no. 2, pp. 87-126, Feb. 2006.

[74] H. Morkoç, Handbook of Nitride Semiconductors and Devices, vol. 3: Physics and Technology of GaN Based Optical and Electronic Devices, Wiley, Weinheim, 2009.

[75] A. Grebene and S. Ghandhi, "General theory for pinched operation of the junction-gate FET," *Journal of Solid-State Electronics*, vol. 12, no. 7, pp. 573-589, July 1969.

[76] J. Chung, E. Piner, and T. Palacios, "N-face GaN/AlGaN HEMTs fabricated through layer transfer technology," *IEEE Electron Device Letters*, vol. 30, no. 2, pp. 113–116, Feb. 2009.

[77] D. Bednarczyk and J. Bednarczyk, "The approximation of the Fermi-Dirac integral $\mathcal{F}_{\frac{1}{2}}(\eta)$," *Physics letters A*, vol. 64, no. 4, pp. 409-410, Jan. 1978.

[78] M. Moradi, Analytical Modeling of Drain-Current Characteristics of AlGaN/GaN HFETs with Incorporation of the Impacts of Virtual-Gate and Transferred-Electron Effect, MASc Thesis, Concordia University, May 2010.

Appendix A: Material parameters redefinition of GaAs as GaN and AlGaAs as AlGaN

A-a Material parameters redefinition of GaAs as GaN

$material parameters redefinition of GaAs to be GaN

Material GAAS

+ permitti=9.7

+ eg.model=1

+ affinity=3.1

+ eg300=3.47

+ egalph=7.7E-4

+ egbeta=600

+ eggamm=0

+ nc300=2.23e18

+ nc.f=1.5

+ nv300=4.6e19

+ nv.f=1.5

+ gcb=2

+ gvb=2

+ edb=0.012

+ eab=0.140

+ taun0=1e-10

+ nsrhn=1

+ an=1

+ bn=0

+ cn=0

+ en=0

+ taup0=8.7e-9

+ nsrhp=1

+ ap=1

+ bp=0

+ cp=0

+ ep=0

+ etrap=0

+ m.rtun=0.25

+ b.rtun=0

+ s.rtun=2

+ e.rtun=0.1

+ c.direct=0

+ augn=0

+ augp=0

+ arichn=24

+ arichp=120

+ n0.bgn=1e17

+ v0.bgn=0

+ con.bgn=0

+ a.ehs=0

+ b.ehs=0

+ c.ehs=0

+ n.ioniza=5e6

+ ecn.ii=1e7

+ exn.ii=1.65

+ p.ioniza=1.1e6

+ ecp.ii=1e7

+ exp.ii=1.32

+ lamhn=1

+ lamrn=1

+ lamhp=1

+ lamrp=1

+ a.fn=0

+ b.fn=0

+ ele.cq=1

+ ele.tauw=1e-12

+ hol.cq=1

+ hol.tauw=1e-12

+ density=6.15e-3

+ dn.lat=1

+ dp.lat=1

+ a.sp.hea=181.5

+ b.sp.hea=0.8225

+ c.sp.hea=-0.00135

+ d.sp.hea=0

+ f.sp.hea=7.5e-7

+ g.sp.hea=0

+ a.th.con=0.68

+ b.th.con=5e-4

+ c.th.con=2e-7

+ d.th.con=0

+ e.th.con=0

+ op.ph.en=0.089

+ lan300=2e-8

+ lap300=2e-8

+ el.emas=0.2

+ ho.emas=1

Mobility GAAS

+ fldmob=2

+ e0n=150e3

+ mun.min=0

+ mun.max=400

+ nrefn=1.69e17

+ nun=0

+ xin=0

+ alphan=0.75

+ gsurfn=1

+ ecn.mu=1e8

+ vsatp=4.7e6

+ vsatn=1.32e7

+ exn1.gaa=4.15

+ exn2.gaa=4.15

+ e0p=500e3

+ mup.min=0

+ mup.max=200

+ nrefp=1e17

+ nup=0

+ xip=0

+ alphap=0.75

+ gsurfp=1

+ ecp.mu=1e8

A-b Material parameters redefinition of AlGaAs as AlGaN

$material parameters redefinition of AlGaAs to be AlGaN

Material ALGAAS

+ affinity=3.1

+ af.x1=-2.85

+ eg.x1=2.73

+ eg300=3.47

+ permitti=9.7

+ eg.model=4

+ eg.x2=0

+ af.x2=0

```
+ nc300=2.23e18
+ nv300=4.6e19
+ gcb=2
+ gvb=2
+ edb=0.012
+ eab=0.140
+ taun0=1e-10
+ nsrhn=1
+ an=1
+ bn=0
+ cn=0
+ en=0
+ taup0=8.7e-9
+ nsrhp=1
+ ap=1
+ bp=0
+ cp=0
+ ep=0
+ etrap=0
+ m.rtun=0.25
+ b.rtun=0
+ s.rtun=2
+ e.rtun=0.1
+ c.direct=0
+ augn=0
```

```
+ augp=0
+ arichn=24
+ arichp=120
+ n0.bgn=1e17
+ v0.bgn=0
+ con.bgn=0
+ a.ehs=0
+ b.ehs=0
+ c.ehs=0
+ n.ioniza=5e6
+ p.ioniza=1.1e6
+ ecn.ii=1e7
+ ecp.ii=1e7
+ cn.iilam=1
+ cp.iilam=1
+ exn.ii=1.65
+ exp.ii=1.32
+ lamhn=1
+ lamrn=1
+ lamhp=1
+ lamrp=1
+ a.fn=0
+ b.fn=0
+ ele.cq=1
+ ele.tauw=1e-12
```

+ hol.cq=1

+ hol.tauw=1e-12

+ density=6.15e-3

+ dn.lat=1

+ dp.lat=1

+ a.sp.hea=181.5

+ b.sp.hea=0.8225

+ c.sp.hea=-0.00135

+ d.sp.hea=0

+ f.sp.hea=7.5e-7

+ g.sp.hea=0

+ a.th.con=0.68

+ b.th.con=5e-4

+ c.th.con=2e-7

+ d.th.con=0

+ e.th.con=0

+ op.ph.en=0.089

+ lan300=2e-8

+ lap300=2e-8

+ el.emas=0.2

+ ho.emas=1

Mobility ALGAAS

+ fldmob=2

+ e0n=150e3

+ mun.min=0

+ mun.max=400

+ nrefn=3.63e17

+ nun=0

+ xin=0

+ alphan=0.75

+ gsurfn=1

+ ecn.mu=1e8

+ vsatp=4.7e6

+ vsatn=1.32e7

+ exn1.gaa=4.15

+ exn2.gaa=4.15

+ e0p=500e3

+ mup.min=0

+ mup.max=200

+ nrefp=1e17

+ nup=0

+ xip=0

+ alphap=0.75

+ gsurfp=1

+ ecp.mu=1e8

+ min.x1=-0.96

+ min.x2=0

+ man.x1=-0.97

+ man.x2=0

+ mip.x1=-0.96

+ mip.x2=0

+ map.x1=-0.78

+ map.x2=0

+ nrefn2=1.75e18

+ nrefp2=1e30

Appendix B: Medici input files of simulation

B-a File: 1

```
TITLE      AlGaN/GaN HFET before stress.
COMMNET    ==================================================
COMMENT    The following part defines device parameters.
ASSIGN     name=Body.tks       n.value=0.68
ASSIGN     name=InGa.tks       n.value=0.002
ASSIGN     name=AGN1.tks       n.value=0.015
ASSIGN     name=AGN2.tks       n.value=0.0025
ASSIGN     name=GaN.tks        n.value=0.025
ASSIGN     name=chan.lgt       n.value=.25
ASSIGN     name=tot.lgt        n.value=25
ASSIGN     name=sds.lgt        n.value=3.75
ASSIGN     name=Body.dop       n.value=1e5
ASSIGN     name=InGa.dop       n.value=1e15
ASSIGN     name=AGN1.dop       n.value=6e17
ASSIGN     name=AGN2.dop       n.value=1e16
ASSIGN     name=GaN.dop        n.value=1e20
COMMENT    ==========================================
COMMENT    The following part generates the mesh structure of the device.
MESH       nx=40 ny=60 virtual smooth.k=1
X.MESH node=1      location=0
X.MESH node=5      location=(@tot.lgt-@chan.lgt-@sds.lgt)*0.5
```

```
X.MESH node=15      location=(@tot.lgt-@chan.lgt)*0.5

X.MESH node=25      location=(@tot.lgt-@chan.lgt)*0.5+@chan.lgt

X.MESH node=35      location=(@tot.lgt+@chan.lgt+@sds.lgt)*0.5

X.MESH node=40      location=@tot.lgt


Y.MESH node=1       location=0

Y.MESH node=9       location=@GaN.tks

Y.MESH node=30      location=@GaN.tks+@AGN1.tks

Y.MESH node=40      location=@GaN.tks+@AGN1.tks+@AGN2.tks

Y.MESH node=50      location=@GaN.tks+@AGN1.tks+@AGN2.tks+@InGa.tks

Y.MESH node=60      location=@GaN.tks+@AGN1.tks+@AGN2.tks+@InGa.tks

+@Body.tks


COMMENT   ==========================================================

COMMENT   The following part determines the material used in different

COMMENT   regions of the device.

REGION        name=s-ohmic    ix.low=1       ix.high=5      iy.low=1

+ iy.high=9      GAAS

REGION name=d-ohmic    ix.low=35      ix.high=40      iy.low=1

+ iy.high=9       GAAS

REGION name=barrier1    ix.low=1      ix.high=40      iy.low=9

+ iy.high=30      AlGAAS x.mole=0.13

REGION name=barrier2    ix.low=1       ix.high=40      iy.low=30

+ iy.high=40      ALGAAS x.mole=0.13

REGION name=channel   ix.low=1       ix.high=40      iy.low=40
```

```
+ iy.high=50      GAAS
REGION name=substra    ix.low=1        ix.high=40      iy.low=50
+ iy.high=60     GAAS
REGION name=isol1       ix.low=5       ix.high=15      iy.low=1
+ iy.high=9       insulato
REGION name=isol2       ix.low=15       ix.high=25      iy.low=1
+ iy.high=9       insulato
REGION name=isol3       ix.low=25       ix.high=35      iy.low=1
+ iy.high=9       insulato

COMMENT    =========================================
COMMENT    The following specifies the location of contact electrodes.
ELECTRODE   name=source ix.l=2  ix.h=4  iy.l=1   iy.h=1
ELECTRODE   name=drain ix.l=37 ix.h=39 iy.l=1   iy.h=1
ELECTRODE   name=gate   ix.l=15 ix.h=25 iy.l=9  iy.h=9
ELECTRODE   name=sub   ix.l=1 ix.h=40   iy.l=60  iy.h=60

COMMENT    ===========================================
COMMENT    The following specifies the doping of each region.
PROFILE       region=s-ohmic n-type x.min=0
+ x.max=(@tot.lgt-@chan.lgt-@sds.lgt)*0.5 y.min=0 y.max=@GaN.tks
+ Uniform n.peak=@GaN.dop
PROFILE region=d-ohmic n-type
+ x.min=(@tot.lgt @chan.lgt)*0.5+@chan.lgt+@sds.lgt*0.5
+ x.max=@tot.lgt  y.min=0      y.max=@GaN.tks    uniform    n.peak=@GaN.dop
```

```
PROFILE region=barrier1 n-type x.min=0 x.max=@tot.lgt
+ y.min=@GaN.tks y.max=@GaN.tks+@AGN1.tks   uniform n.peak=@AGN1.dop
PROFILE region=barrier2 n-type x.min=0 x.max=@tot.lgt
+ y.min=@GaN.tks+@AGN1.tks y.max=@GaN.tks+@AGN1.tks+@AGN2.tks uniform
+ n.peak=@AGN2.dop
PROFILE region=channel n-type x.min=0 x.max=@tot.lgt
+ y.min=@GaN.tks+@AGN1.tks+@AGN2.tks
+ y.max=@GaN.tks+@AGN1.tks+@AGN2.tks+@InGa.tks
+ uniform  n.peak=@InGa.dop
PROFILE region=substra n-type x.min=0 x.max=@tot.lgt
+ y.min=@GaN.tks+@AGN1.tks+@AGN2.tks+@InGa.tks
+ y.max=@GaN.tks+@AGN1.tks+@AGN2.tks+@InGa.tks+@Body.tks uniform
+ n.peak=@Body.dop
 PROFILE   n.type  conc=3.1E20
+ y.min=@GaN.tks+@AGN1.tks+@agn2.tks+@InGa.tks*0.5
+ char=@InGa.tks*0.02
INTERFACE region=(barrier2,channel) QF=1E13
PLOT.2D grid fill scale

COMMENT   =========================================
COMMENT   Material parameters redifinition of AlGaAs to be AlGaN.
CALL file=dataGaNupdate18809.inp
CALL file=dataAlGaNupdate18809.inp
CONTACT   name=gate SCHOTTKY WORKf=5.17
SAVE     MESH OUT.F=MES.MSH
```

```
MODELS    fermi auger consrh analytic fldmob hjtem hjtun
COMMENT   ===========
COMMENT   Initial solution.
SYMB      NEWT CARR=0
SOLVE     V(sub)=0 V(source)=0 V(drain)=0.05  V(gate)=0
SYMB      NEWT CARR=2
METHOD    itlimit=60 px.toler=1e-3 cx.toler=1e-4
SOLVE
PLOT.1D   X.ST=(@tot.lgt-@chan.lgt)*0.5+@chan.lgt/2
+ X.END=(@tot.lgt-@chan.lgt)*0.5+@chan.lgt/2
+ Y.ST=0 Y.EN=@GaN.tks+@AGN1.tks+@AGN2.tks+@InGa.tks+@Body.tks
+ DOPING LOG
+ bottom=1e2 top=1e22 left=0
+ right=@GaN.tks+@AGN1.tks+@AGN2.tks+@InGa.tks+@Body.tks
+ TITLE=" Channel Doping & Electrons Device ON"
PLOT.1D   X.ST=(@tot.lgt-@chan.lgt)*0.5+@chan.lgt/2
+ X.END=(@tot.lgt-@chan.lgt)*0.5+@chan.lgt/2
+ Y.ST=@GaN.tks+@AGN1.tks+@AGN2.tks
+ Y.EN=@GaN.tks+@AGN1.tks+@AGN2.tks+@InGa.tks
+ ELECT LOG    COL=2
LABEL LABEL=Electrons COL=2 X=.8 Y=1e8
LABEL LABEL=Doping X=.02 Y=1e17
PLOT.1D X.ST=(@tot.lgt-@chan.lgt)*0.5+@chan.lgt/2
+ X.END=(@tot.lgt-@chan.lgt)*0.5+@chan.lgt/2
+ Y.ST=0 Y.EN=@GaN.tks+@AGN1.tks+@AGN2.tks+@InGa.tks+@Body.tks
```

```
+ COND TOP=2.5 BOT=-5
+ NEG TITLE="HFET Band structure Device ON"
PLOT.1D   X.ST=(@tot.lgt-@chan.lgt)*0.5+@chan.lgt/2
+ X.END=(@tot.lgt-@chan.lgt)*0.5+@chan.lgt/2
+ Y.ST=0 Y.EN=@GaN.tks+@AGN1.tks+@AGN2.tks+@InGa.tks+@Body.tks
+ VAL UNCH NEG
PLOT.1D   X.ST=(@tot.lgt-@chan.lgt)*0.5+@chan.lgt/2
+ X.END=(@tot.lgt-@chan.lgt)*0.5+@chan.lgt/2
+ Y.ST=0 Y.EN=@GaN.tks+@AGN1.tks+@AGN2.tks+@InGa.tks+@Body.tks
+ QFN   UNCH NEG COL=2
LABEL     LABEL=Cond X=0.1  Y=1
LABEL     LABEL=Qfn X=0.1  Y=0
LABEL     LABEL=Val X=0.1  Y=-3
PLOT.1D X.ST=(@tot.lgt-@chan.lgt)*0.5+@chan.lgt*1/3
+ X.END=(@tot.lgt-@chan.lgt)*0.5+@chan.lgt*1/3
+ Y.ST=0 Y.EN=@GaN.tks+@AGN1.tks+@AGN2.tks+@InGa.tks+@Body.tks
+ COND TOP=2.5 BOT=-5
+ NEG TITLE="HFET Band structure Device ON"
PLOT.1D   X.ST=(@tot.lgt-@chan.lgt)*0.5+@chan.lgt*1/3
+ X.END=(@tot.lgt-@chan.lgt)*0.5+@chan.lgt*1/3
+ Y.ST=0 Y.EN=@GaN.tks+@AGN1.tks+@AGN2.tks+@InGa.tks+@Body.tks
+ VAL UNCH NEG
PLOT.1D   X.ST=(@tot.lgt-@chan.lgt)*0.5+@chan.lgt*1/3
+ X.END=(@tot.lgt-@chan.lgt)*0.5+@chan.lgt*1/3
+ Y.ST=0 Y.EN=@GaN.tks+@AGN1.tks+@AGN2.tks+@InGa.tks+@Body.tks
```

```
+ QFN   UNCH NEG COL=2
LABEL     LABEL=Cond X=0.1  Y=1
LABEL     LABEL=Qfn X=0.1  Y=0
LABEL     LABEL=Val X=0.1  Y=-3
PLOT.1D X.ST=(@tot.lgt-@chan.lgt)*0.5+@chan.lgt*2/3
+ X.END=(@tot.lgt-@chan.lgt)*0.5+@chan.lgt*2/3
+ Y.ST=0 Y.EN=@GaN.tks+@AGN1.tks+@AGN2.tks+@InGa.tks+@Body.tks
+ COND TOP=2.5 BOT=-5
+ NEG TITLE="HFET Band structure Device ON"
PLOT.1D   X.ST=(@tot.lgt-@chan.lgt)*0.5+@chan.lgt*2/3
+ X.END=(@tot.lgt-@chan.lgt)*0.5+@chan.lgt*2/3
+ Y.ST=0 Y.EN=@GaN.tks+@AGN1.tks+@AGN2.tks+@InGa.tks+@Body.tks
+ VAL   UNCH NEG
PLOT.1D X.ST=(@tot.lgt-@chan.lgt)*0.5+@chan.lgt*2/3
+ X.END=(@tot.lgt-@chan.lgt)*0.5+@chan.lgt*2/3
+Y.ST=0 Y.EN=@GaN.tks+@AGN1.tks+@AGN2.tks+@InGa.tks+@Body.tks
+ QFN UNCH NEG COL=2
LABEL     LABEL=Cond X=0.1  Y=1
LABEL     LABEL=Qfn X=0.1  Y=0
LABEL     LABEL=Val X=0.1  Y=-3
PLOT.1D X.ST=(@tot.lgt-@chan.lgt)*0.25
+ X.END=(@tot.lgt-@chan.lgt)*0.25
+ Y.ST=0 Y.EN=@GaN.tks+@AGN1.tks+@AGN2.tks+@InGa.tks+@Body.tks
+ COND TOP=2.5 BOT=-5
+ NEG TITLE="HFET Band structure Device ON"
```

```
PLOT.1D   X.ST=(@tot.lgt-@chan.lgt)*0.25
+ X.END=(@tot.lgt-@chan.lgt)*0.25
+ Y.ST=0 Y.EN=@GaN.tks+@AGN1.tks+@AGN2.tks+@InGa.tks+@Body.tks
+ VAL UNCH NEG
PLOT.1D   X.ST=(@tot.lgt-@chan.lgt)*0.25
+ X.END=(@tot.lgt-@chan.lgt)*0.25
+ Y.ST=0 Y.EN=@GaN.tks+@AGN1.tks+@AGN2.tks+@InGa.tks+@Body.tks
+ QFN   UNCH NEG COL=2
PLOT.1D X.ST=@tot.lgt-(@tot.lgt-@chan.lgt)*0.25
+ X.END=@tot.lgt-(@tot.lgt-@chan.lgt)*0.25
+ Y.ST=0 Y.EN=@GaN.tks+@AGN1.tks+@AGN2.tks+@InGa.tks+@Body.tks
+ COND TOP=2.5 BOT=-5
+ NEG TITLE="HFET Band structure Device ON"
PLOT.1D   X.ST=@tot.lgt-(@tot.lgt-@chan.lgt)*0.25
+ X.END=@tot.lgt-(@tot.lgt-@chan.lgt)*0.25
+ Y.ST=0 Y.EN=@GaN.tks+@AGN1.tks+@AGN2.tks+@InGa.tks+@Body.tks
+ VAL UNCH NEG
PLOT.1D X.ST=@tot.lgt-(@tot.lgt-@chan.lgt)*0.25
+ X.END=@tot.lgt-(@tot.lgt-@chan.lgt)*0.25
+ Y.ST=0 Y.EN=@GaN.tks+@AGN1.tks+@AGN2.tks+@InGa.tks+@Body.tks
+ QFN UNCH NEG COL=2
PLOT.2D grid fill
COMMENT   =====================
COMMENT   Generate plot of device structure.
PLOT.2D BOUNDARY FILL
```

```
+ TITLE="HFET Current Flow, Device ON"
FILL     REGION=channel COLOR=5
FILL     REGION=barrier1 COLOR=2
FILL     REGION=barrier2 COLOR=6
FILL     REGION=s-ohmic COLOR=3
FILL     REGION=d-ohmic COLOR=3
FILL     REGION=substra COLOR=9
FILL     REGION=isol1 COLOR=11
FILL     REGION=isol2 COLOR=7
FILL     REGION=isol3 COLOR=11

LABEL    LABEL=AlGaN x=.5 y=.1
LABEL    LABEL=GaN x=.1 y=.003
LABEL    LABEL=GaN x=.9 y=.003
LABEL    LABEL=PASSIVATION x=.425 y=.003
LABEL    LABEL=AlGaN x=.5 y=.04
LABEL    LABEL=GaN x=.5 y=.055
LABEL    LABEL=AlGaN x=.5 y=.05
CONTOUR   FLOW
SOLVE V(sub)=0 V(source)=0 V(drain)=2.5  V(gate)=-1.8
PLOT.1D x.ax=j.field y.ax=ele.vel points ^order
PLOT.1D ele.vel x.start=(@tot.lgt-@chan.lgt-@sds.lgt)*0.5
+ x.end=(@tot.lgt+@chan.lgt+@sds.lgt)*0.5
+ y.start=@GaN.tks+@AGN1.tks+@AGN2.tks+(@InGa.tks*0.5)
+ y.end=@GaN.tks+@AGN1.tks+@AGN2.tks+(@InGa.tks*0.5)
```

```
+ print out.file=velocity4.dat
plot.1d j.efield x.start=(@tot.lgt-@chan.lgt-@sds.lgt)*0.5
+ x.end=(@tot.lgt+@chan.lgt+@sds.lgt)*0.5
+ y.start=@GaN.tks+@AGN1.tks+@AGN2.tks+(@InGa.tks*0.5)
+ y.end=@GaN.tks+@AGN1.tks+@AGN2.tks+(@InGa.tks*0.5)
+ print out.file=electricfield4.dat
SOLVE    V(drain)=0.05  V(gate)=-1.8
+ ELEC=drain VSTEP=.4 NSTEP=37
PLOT.1D X.AX=V(drain) Y.AX=I(drain) points ^order print out.file=bit18.dat
SOLVE V(drain)=14.85 V(gate)=-2.2
+ ELEC=drain VSTEP=-.4 NSTEP=37
PLOT.1D   X.AX=V(drain)  Y.AX=I(drain)   points  ^order  unchange  print
+ out.file=bit22.dat
SOLVE    V(drain)=0.05  V(gate)=-2.6
+    ELEC=drain VSTEP=.4 NSTEP=37
PLOT.1D   X.AX=V(drain)  Y.AX=I(drain)   points   ^order  unchange print
+ out.file=bit26.dat
SOLVE V(drain)=14.85    V(gate)=-3
+    ELEC=drain VSTEP=-.4 NSTEP=37
PLOT.1D   X.AX=V(drain)  Y.AX=I(drain)  points   ^order unchange print
+ out.file=bit3.dat
SOLVE    V(drain)=0.05  V(gate)=-3.4
+    ELEC=drain VSTEP=.4 NSTEP=37
PLOT.1D   X.AX=V(drain)  Y.AX=I(drain)   points   ^order  unchange print
+ out.file=bit34.dat
```

B-b File: 2

```
TITLE       AlGaN/GaN HFET after stress.

COMMENT     ================================

COMMENT     The following part defines device parameters.

ASSIGN      name=Body.tks       n.value=0.68

ASSIGN      name=InGa.tks       n.value=0.002

ASSIGN      name=AGN1.tks       n.value=0.015

ASSIGN      name=AGN2.tks       n.value=0.0025

ASSIGN      name=GaN.tks        n.value=0.025

ASSIGN      name=trap.tks       n.value=0.011


ASSIGN      name=chan.lgt       n.value=.25

ASSIGN      name=tot.lgt        n.value=25

ASSIGN      name=sds.lgt        n.value=3.75

ASSIGN      name=trap.lgt       n.value=0.056


ASSIGN      name=Body.dop       n.value=1e5

ASSIGN      name=InGa.dop       n.value=1e15

ASSIGN      name=AGN1.dop       n.value=6e17

ASSIGN      name=AGN2.dop       n.value=1e16

ASSIGN      name=GaN.dop        n.value=1e20
```

```
ASSIGN        name=trap.dop          n.value=1e15


COMMENT   =========================================

COMMENT   The following part generates the mesh structure of the device.

MESH nx=40 ny=60 virtual smooth.k=1

X.MESH node=1       location=0

X.MESH node=5       location=(@tot.lgt-@chan.lgt-@sds.lgt)*0.5

X.MESH node=15      location=(@tot.lgt-@chan.lgt)*0.5

X.MESH node=25      location=(@tot.lgt-@chan.lgt)*0.5+@chan.lgt

X.MESH node=30      location=(@tot.lgt+@chan.lgt)*0.5+@trap.lgt

X.MESH node=35      location=(@tot.lgt+@chan.lgt+@sds.lgt)*0.5

X.MESH node=40      location=@tot.lgt


Y.MESH node=1       location=0

Y.MESH node=5       location=@GaN.tks-@trap.tks

Y.MESH node=9       location=@GaN.tks

Y.MESH node=30      location=@GaN.tks+@AGN1.tks

Y.MESH node=40      location=@GaN.tks+@AGN1.tks+@AGN2.tks

Y.MESH node=50      location=@GaN.tks+@AGN1.tks+@AGN2.tks+@InGa.tks

Y.MESH node=60     location=@GaN.tks+@AGN1.tks

+@AGN2.tks+@InGa.tks+@Body.tks
```

```
COMMENT   ========================================
COMMENT   The following part determines the material used in different
COMMENT   regions of the device.
REGION name=s-ohmic    ix.low=1       ix.high=5   iy.low=1
+         iy.high=9         GAAS
REGION name=d-ohmic    ix.low=35      ix.high=40      iy.low=1
+         iy.high=9        GAAS
REGION name=barrier1    ix.low=1       ix.high=40      iy.low=9
+         iy.high=30       AlGAAS X.MOLE=0.15
REGION name=barrier2    ix.low=1        ix.high=40      iy.low=30
+         iy.high=40       ALGAAS X.MOLE=0.15
REGION name=channel   ix.low=1        ix.high=40      iy.low=40
+         iy.high=50       GAAS
REGION name=substra    ix.low=1        ix.high=40      iy.low=50
+         iy.high=60      GAAS
REGION name=isol1       ix.low=5       ix.high=15      iy.low=1
+         iy.high=9        insulato
REGION name=isol11       ix.low=15       ix.high=25      iy.low=1
+         iy.high=9        insulato
REGION name=isol2      ix.low=30 ix.high=35 iy.low=1
+         iy.high=9 insulato
```

```
REGION name=isol3 ix.low=25 ix.high=30 iy.low=1
+         iy.high=5     insulato


REGION name=trap ix.low=25 ix.high=30 iy.low=5
+         iy.high=9 insulato
COMMENT    ==========================================
COMMENT    The following specifies the location of contact electrodes.


ELECTRODE name=source ix.l=2    ix.h=4  iy.l=1   iy.h=1
ELECTRODE name=drain ix.l=37 ix.h=39 iy.l=1    iy.h=1
ELECTRODE name=gate   ix.l=15 ix.h=25  iy.l=9    iy.h=9
ELECTRODE name=sub   ix.l=1 ix.h=40     iy.l=60  iy.h=60



COMMENT    ====================================
COMMENT    The following specifies the doping of each region.


PROFILE        region=s-ohmic n-type x.min=0
+ x.max=(@tot.lgt-@chan.lgt-@sds.lgt)*0.5
+ y.min=0       y.max=@GaN.tks    uniform       n.peak=@GaN.dop
PROFILE region=d-ohmic n-type
+ x.min=(@tot.lgt-@chan.lgt)*0.5+@chan.lgt+@sds.lgt*0.5
+ x.max=@tot.lgt y.min=0      y.max=@GaN.tks    uniform    n.peak=@GaN.dop
```

```
PROFILE region=barrier1 n-type x.min=0 x.max=@tot.lgt
+ y.min=@GaN.tks y.max=@GaN.tks+@AGN1.tks   uniform  n.peak=@AGN1.dop
PROFILE region=barrier2 n-type x.min=0 x.max=@tot.lgt
+ y.min=@GaN.tks+@AGN1.tks y.max=@GaN.tks+@AGN1.tks+@AGN2.tks  uniform
+ n.peak=@AGN2.dop
 PROFILE region=channel n-type x.min=0 x.max=@tot.lgt
+ y.min=@GaN.tks+@AGN1.tks+@AGN2.tks
+ y.max=@GaN.tks+@AGN1.tks+@AGN2.tks+@InGa.tks
+ uniform n.peak=@InGa.dop
PROFILE region=substra n-type x.min=0 x.max=@tot.lgt
+ y.min=@GaN.tks+@AGN1.tks+@AGN2.tks+@InGa.tks
+ y.max=@GaN.tks+@AGN1.tks+@AGN2.tks+@InGa.tks+@Body.tks uniform
+ n.peak=@Body.dop
PROFILE region=trap n-type x.min=(@tot.lgt+@chan.lgt)*0.5
+ x.max=(@tot.lgt+@chan.lgt)*0.5+@trap.lgt
+ y.min=@GaN.tks-@trap.tks y.max=@Gan.tks uniform
+ n.peak=@trap.dop
PROFILE   N.TYPE  CONC=2.98E20 Y.MIN=@GaN.tks+@AGN1.tks+@InGa.tks*0.4
+ char=@agn2.tks*0.05
INTERFACE region=(barrier2,channel) QF=1E13
INTERFACE region=(trap,barrier1) QF=-5.5e14
PLOT.2D grid fill scale
```

```
COMMENT   ==========================================

COMMENT   Material parameters redifinition of AlGaAs to be AlGaN.

CALL file=dataGaNupdate18809.inp

CALL file=dataAlGaNupdate18809.inp

CONTACT   name=gate SCHOTTKY WORKf=5.17

SAVE      MESH OUT.F=MES.MSH

MODELS    fermi auger consrh  analytic fldmob hjtem hjtun


COMMENT   ==========

COMMENT   Initial solution.

SYMB      NEWT  CARR=0

SOLVE     V(sub)=0 V(source)=0 V(drain)=0.05  V(gate)=0

SYMB      NEWT CARR=2

METHOD    itlimit=60 px.toler=1e-1 cx.toler=1e-1

SOLVE

PLOT.1D   X.ST=(@tot.lgt-@chan.lgt)*0.5+@chan.lgt/2

+X.END=(@tot.lgt-@chan.lgt)*0.5+@chan.lgt/2

+Y.ST=0 Y.EN=@GaN.tks+@AGN1.tks+@AGN2.tks+@InGa.tks+@Body.tks

+ DOPING LOG

+   bottom=1e2 top=1e22 left=0

+   right=@GaN.tks+@AGN1.tks+@AGN2.tks+@InGa.tks+@Body.tks

+   TITLE=" Channel Doping & Electrons Device ON"
```

```
PLOT.1D   X.ST=(@tot.lgt-@chan.lgt)*0.5+@chan.lgt/2
+ X.END=(@tot.lgt-@chan.lgt)*0.5+@chan.lgt/2
+ Y.ST=@GaN.tks+@AGN1.tks+@AGN2.tks
+ Y.EN=@GaN.tks+@AGN1.tks+@AGN2.tks+@InGa.tks
+ ELECT LOG    COL=2
LABEL     LABEL=Electrons COL=2 X=.8 Y=1e8
LABEL     LABEL=Doping X=.02 Y=1e17
PLOT.1D X.ST=(@tot.lgt-@chan.lgt)*0.5+@chan.lgt/2
+ X.END=(@tot.lgt-@chan.lgt)*0.5+@chan.lgt/2
+ Y.ST=0 Y.EN=@GaN.tks+@AGN1.tks+@AGN2.tks+@InGa.tks+@Body.tks
+ COND TOP=2.5 BOT=-5
+ NEG TITLE="HFET Band structure Device ON"
PLOT.1D   X.ST=(@tot.lgt-@chan.lgt)*0.5+@chan.lgt/2
+X.END=(@tot.lgt-@chan.lgt)*0.5+@chan.lgt/2
+Y.ST=0 Y.EN=@GaN.tks+@AGN1.tks+@AGN2.tks+@InGa.tks+@Body.tks
+ VAL UNCH NEG
PLOT.1D   X.ST=(@tot.lgt-@chan.lgt)*0.5+@chan.lgt/2
+ X.END=(@tot.lgt-@chan.lgt)*0.5+@chan.lgt/2
+ Y.ST=0 Y.EN=@GaN.tks+@AGN1.tks+@AGN2.tks+@InGa.tks+@Body.tks
+ QFN UNCH NEG COL=2
LABEL     LABEL=Cond X=0.1 Y=1
LABEL     LABEL=Qfn X=0.1  Y=0
LABEL     LABEL=Val X=0.1  Y=-3
```

```
PLOT.1D X.ST=(@tot.lgt-@chan.lgt)*0.5+@chan.lgt*1/3
+ X.END=(@tot.lgt-@chan.lgt)*0.5+@chan.lgt*1/3
+ Y.ST=0 Y.EN=@GaN.tks+@AGN1.tks+@AGN2.tks+@InGa.tks+@Body.tks
+ COND TOP=2.5 BOT=-5
+ NEG TITLE="HFET Band structure Device ON"
PLOT.1D   X.ST=(@tot.lgt-@chan.lgt)*0.5+@chan.lgt*1/3
+ X.END=(@tot.lgt-@chan.lgt)*0.5+@chan.lgt*1/3
+ Y.ST=0 Y.EN=@GaN.tks+@AGN1.tks+@AGN2.tks+@InGa.tks+@Body.tks
+ VAL UNCH NEG
PLOT.1D   X.ST=(@tot.lgt-@chan.lgt)*0.5+@chan.lgt*1/3
+ X.END=(@tot.lgt-@chan.lgt)*0.5+@chan.lgt*1/3
+ Y.ST=0 Y.EN=@GaN.tks+@AGN1.tks+@AGN2.tks+@InGa.tks+@Body.tks
+ QFN UNCH NEG COL=2
LABEL     LABEL=Cond X=0.1 Y=1
LABEL     LABEL=Qfn X=0.1  Y=0
LABEL     LABEL=Val X=0.1  Y=-3
PLOT.1D X.ST=(@tot.lgt-@chan.lgt)*0.5+@chan.lgt*2/3
+ X.END=(@tot.lgt-@chan.lgt)*0.5+@chan.lgt*2/3
+ Y.ST=0 Y.EN=@GaN.tks+@AGN1.tks+@AGN2.tks+@InGa.tks+@Body.tks
+ COND TOP=2.5 BOT=-5
+ NEG TITLE="HFET Band structure Device ON"
PLOT.1D   X.ST=(@tot.lgt-@chan.lgt)*0.5+@chan.lgt*2/3
+X.END=(@tot.lgt-@chan.lgt)*0.5+@chan.lgt*2/3
```

```
+Y.ST=0 Y.EN=@GaN.tks+@AGN1.tks+@AGN2.tks+@InGa.tks+@Body.tks
+VAL UNCH NEG
PLOT.1D   X.ST=(@tot.lgt-@chan.lgt)*0.5+@chan.lgt*2/3
+ X.END=(@tot.lgt-@chan.lgt)*0.5+@chan.lgt*2/3
+ Y.ST=0 Y.EN=@GaN.tks+@AGN1.tks+@AGN2.tks+@InGa.tks+@Body.tks
+ QFN UNCH NEG COL=2
LABEL     LABEL=Cond X=0.1 Y=1
LABEL     LABEL=Qfn X=0.1  Y=0
LABEL     LABEL=Val X=0.1  Y=-3
PLOT.1D X.ST=(@tot.lgt-@chan.lgt)*0.25
+ X.END=(@tot.lgt-@chan.lgt)*0.25
+ Y.ST=0 Y.EN=@GaN.tks+@AGN1.tks+@AGN2.tks+@InGa.tks+@Body.tks
+ COND TOP=2.5 BOT=-5
+ NEG TITLE="HFET Band structure Device ON"
PLOT.1D   X.ST=(@tot.lgt-@chan.lgt)*0.25
+ X.END=(@tot.lgt-@chan.lgt)*0.25
+ Y.ST=0 Y.EN=@GaN.tks+@AGN1.tks+@AGN2.tks+@InGa.tks+@Body.tks
+ VAL UNCH NEG
PLOT.1D X.ST=(@tot.lgt-@chan.lgt)*0.25
+ X.END=(@tot.lgt-@chan.lgt)*0.25
+ Y.ST=0 Y.EN=@GaN.tks+@AGN1.tks+@AGN2.tks+@InGa.tks+@Body.tks
+ QFN UNCH NEG COL=2
PLOT.1D X.ST=@tot.lgt-(@tot.lgt-@chan.lgt)*0.25
```

```
+ X.END=@tot.lgt-(@tot.lgt-@chan.lgt)*0.25
+ Y.ST=0 Y.EN=@GaN.tks+@AGN1.tks+@AGN2.tks+@InGa.tks+@Body.tks
+ COND TOP=2.5 BOT=-5
+ NEG TITLE="HFET Band structure Device ON"
PLOT.1D   X.ST=@tot.lgt-(@tot.lgt-@chan.lgt)*0.25
+ X.END=@tot.lgt-(@tot.lgt-@chan.lgt)*0.25
+ Y.ST=0 Y.EN=@GaN.tks+@AGN1.tks+@AGN2.tks+@InGa.tks+@Body.tks
+ VAL UNCH NEG
PLOT.1D   X.ST=@tot.lgt-(@tot.lgt-@chan.lgt)*0.25
+ X.END=@tot.lgt-(@tot.lgt-@chan.lgt)*0.25
+ Y.ST=0 Y.EN=@GaN.tks+@AGN1.tks+@AGN2.tks+@InGa.tks+@Body.tks
+ QFN UNCH NEG COL=2
PLOT.2D grid fill
COMMENT   ======================
COMMENT   Generate plot of device structure.
PLOT.2D         BOUNDARY FILL
+ TITLE="HFET Current Flow, Device ON"
FILL      REGION=channel COLOR=5
FILL      REGION=barrier1 COLOR=2
FILL      REGION=barrier2 COLOR=6
FILL      REGION=s-ohmic COLOR=3
FILL      REGION=d-ohmic COLOR=3
FILL      REGION=substra COLOR=9
```

```
FILL     REGION=isol1 COLOR=11
FILL     REGION=isol11 COLOR=7
FILL     REGION=isol2 COLOR=11
FILL     REGION=isol3 COLOR=11
FILL     REGION=trap COLOR=13

LABEL    LABEL=AlGaN x=.5 y=.1
LABEL    LABEL=GaN x=.1 y=.003
LABEL    LABEL=GaN x=.9 y=.003
LABEL    LABEL=PASSIVATION x=.425 y=.003
LABEL    LABEL=AlGaN x=.5 y=.04
LABEL    LABEL=GaN x=.5 y=.055
LABEL    LABEL=AlGaN x=.5 y=.05
CONTOUR   FLOW
SOLVE    V(sub)=0 V(source)=0 V(drain)=2.5  V(gate)=-1.8
PLOT.1D ele.vel x.start=(@tot.lgt-@chan.lgt-@sds.lgt)*0.5
+ x.end=(@tot.lgt+@chan.lgt+@sds.lgt)*0.5
+ y.start=@GaN.tks+@AGN1.tks+@AGN2.tks
+ (@InGa.tks*0.5)  y.end=@GaN.tks+@AGN1.tks+@AGN2.tks+(@InGa.tks*0.5)
+ print out.file=velocity4.dat
PLOT.1D j.efield x.start=(@tot.lgt-@chan.lgt-@sds.lgt)*0.5
+ x.end=(@tot.lgt+@chan.lgt+@sds.lgt)*0.5
+ y.start=@GaN.tks+@AGN1.tks+@AGN2.tks
```

```
+ (@InGa.tks*0.5)    y.end=@GaN.tks+@AGN1.tks+@AGN2.tks+(@InGa.tks*0.5)

+ print out.file=electricfield4.dat

SOLVE     V(drain)=0.05  V(gate)=-1.8

+ ELEC=drain VSTEP=.4 NSTEP=37

PLOT.1D   X.AX=V(drain)  Y.AX=I(drain)    points ^order   print out.file=bit18.dat

SOLVE     V(drain)=14.85    V(gate)=-2.2

+ ELEC=drain VSTEP=-.4 NSTEP=37

PLOT.1D      X.AX=V(drain)     Y.AX=I(drain)      points     ^order     unchange     print
out.file=bit22.dat

SOLVE     V(drain)=0.05  V(gate)=-2.6

+    ELEC=drain VSTEP=.4 NSTEP=37

PLOT.1D      X.AX=V(drain)     Y.AX=I(drain)      points      ^order     unchange   print
out.file=bit26.dat

SOLVE     V(drain)=14.85    V(gate)=-3

+    ELEC=drain VSTEP=-.4 NSTEP=37

PLOT.1D   X.AX=V(drain)  Y.AX=I(drain)  points   ^order

+ unchange print out.file=bit3.dat

SOLVE     V(drain)=0.05  V(gate)=-3.4

+    ELEC=drain VSTEP=.4 NSTEP=37

PLOT.1D   X.AX=V(drain)  Y.AX=I(drain)   points   ^order

+ unchange print out.file=bit34.dat
```